



**University of  
Zurich**<sup>UZH</sup>

# Opportunities for geomorphological and glaciological research from the Arctic-wide high resolution ArcticDEM

GEO 511 Master's Thesis

**Author**

Julian Stuber  
13-743-109

**Supervised by**

Prof. Dr. Andreas Vieli

**Faculty representative**

Prof. Dr. Ross Purves

31.03.2022

Department of Geography, University of Zurich



University of  
Zurich<sup>UZH</sup>

---

---

OPPORTUNITIES FOR GEOMORPHOLOGICAL AND  
GLACIOLOGICAL RESEARCH FROM THE ARCTIC-WIDE  
HIGH-RESOLUTION ARCTICDEM

---

---

GEO 511 MASTER THESIS

SUBMITTED IN PARTIAL FULFILLMENT OF THE REQUIREMENTS FOR  
THE DEGREE OF MASTER OF SCIENCE IN GEOGRAPHY

AUTHOR

JULIAN STUBER

EGG 24,9216 HELDSWIL, SWITZERLAND

MATRICULATION NUMBER: 13-743-109

EMAIL: [JULIAN.STUBER@UZH.CH](mailto:JULIAN.STUBER@UZH.CH)

SUPERVISORS

PROF. DR. ROSS PURVES

GEOCOMPUTATION

DEPARTMENT OF GEOGRAPHY

UNIVERSITY OF ZURICH

PROF. DR. ANDREAS VIELI

GLACIOLOGY AND GEOMORPHODYNAMICS

DEPARTMENT OF GEOGRAPHY

UNIVERSITY OF ZURICH

DATE OF SUBMISSION: 31.03.2022

## Abstract

The ArcticDEM presents an interesting opportunity for research. By uniting knowledge and methods from geomorphometry and glaciology, this vast data source can help reconstructing features such as eskers, which are found in beds of paleo-ice sheets. This in turn can contribute to a deeper understanding and more accurate models of glacier dynamics. Using a region growing algorithm (Adams and Bischof (1994), Straumann and Purves (2008), Bechtel, Ringeler, and Böhner (2008)) a map of Canadian eskers should be generated and compared to existing work in the same area. The approach presented in this thesis is capable of extracting esker segments as a whole. Within a defined study area in the McCann Lake Area in Northwest Territories, the results show >50% accuracy in regards to a reference map of Canadian eskers. Furthermore, existing recent applications from the ArcticDEM in related research fields are discussed.

## Acknowledgements

First and foremost, I would like to sincerely thank my two supervisors Prof. Dr. Ross Purves and Prof. Dr. Andreas Vieli for their guidance, patience and persistence. I am truly grateful for their inputs and the way they accompanied me throughout the time of writing. Then, my gratitude goes to my family, my girlfriend, friends and colleagues from university. Be it for motivation, proof-reading or sharing their thoughts or simply a meal with me. Thank you.

# Contents

<b>1</b>	<b>Introduction</b>	<b>1</b>
1.1	Motivation . . . . .	1
1.2	Research Questions & Goals . . . . .	2
<b>2</b>	<b>State of Research</b>	<b>3</b>
2.1	Glaciology . . . . .	3
2.1.1	Laurentide Ice Sheet (LIS) . . . . .	4
2.1.2	Subglacial Meltwater Drainage Systems . . . . .	4
2.2	Geomorphometry . . . . .	6
2.2.1	Basic Land-Surface Parameters . . . . .	7
2.2.2	Landforms . . . . .	10
2.2.3	Eskers: Extracting Domain Knowledge about a Landform . . . . .	12
2.3	Seeded Region Growing . . . . .	13
2.4	ArcticDEM . . . . .	14
<b>3</b>	<b>Data and Methods</b>	<b>17</b>
3.1	Data . . . . .	17
3.1.1	ArcticDEM: Elevation Data . . . . .	17
3.1.2	Eskers_Canada.shp: Reference Data on Eskers . . . . .	19
3.2	Methods . . . . .	19
3.2.1	Software . . . . .	20
3.2.2	Study Area . . . . .	20
3.2.3	Download and Preprocessing . . . . .	21

---

3.2.4	Landform Parameterisation . . . . .	24
3.2.5	Finding Ridge Lines . . . . .	24
3.2.6	Seeded Region Growing . . . . .	25
3.2.7	Postprocessing . . . . .	26
3.2.8	Validation . . . . .	27
<b>4</b>	<b>Results</b>	<b>28</b>
4.1	Combination of Morphometric Parameters and Sieving Threshold: Influence on Accuracy	28
4.2	Seed Generation & Ridge Detection . . . . .	29
4.3	Seed Region Growing & Postprocessing . . . . .	30
4.4	Validation of Results . . . . .	31
<b>5</b>	<b>Discussion</b>	<b>35</b>
5.1	Interpretation of Results . . . . .	35
5.1.1	Combination of Morphometric Parameters and Sieving Threshold: Influence on Accuracy . . . . .	35
5.2	Methodological Limitations . . . . .	37
5.2.1	Focus on Geomorphometric Characteristics . . . . .	37
5.2.2	Software Constraints . . . . .	38
5.3	Data Limitations . . . . .	39
5.3.1	ArcticDEM . . . . .	39
5.3.2	Reference Data Set on Eskers . . . . .	39
5.4	Outlook . . . . .	40
<b>6</b>	<b>Conclusion</b>	<b>42</b>
	<b>Appendices</b>	
<b>A</b>	<b>Dictionaries, Data &amp; Software</b>	<b>44</b>

# List of Figures

2.1	Extent of LIS during last glacial maximum, including reconstructed elevation. Elevation values are given in 100's of meters above present-day sea-level. The extent of the LIS (including ice-shelves) at last glacial maximum is derived from Dyke and V. K. Prest (1987). Image and data copied from Lacelle et al. (2018). . . . .	5
2.2	Simplified cross-sections of efficient subglacial drainage channels. Adapted from Davison et al. (2019). . . . .	6
2.3	The spectrum between general and specific geomorphometry, copied from Wood (1996).	7
2.4	curvatures, copied from Peter A. Shary, Sharaya, and Mitusov (2002) . . . . .	9
2.5	Geomorphons for the ten most common landform elements and their 3D- representation in the form of morphometric feature types. Copied from Jasiewicz and Stepinski (2013)	11
2.6	Classification of morphometric feature type and conceptual illustration of a ridge in a grid. . . . .	14
2.7	Eskers accompanied by elongated hummock corridors. Copied from Lewington, Livingstone, Sole, et al. (2019). . . . .	16
3.1	Domain of ArcticDEM, covering all landmass above 60° North, as well as Alaska, Greenland and the Kamchatka Peninsula in their entirety. Extent after latest and final release 7 in 2016. . . . .	18
3.2	Planned conceptual workflow. . . . .	20
3.3	ArcticDEM tile 26_12 located in the McCann Lake Area, North West Territories, Canada. . . . .	22
3.4	Division of tile 26_12 into four sub-tiles. This work focuses on sub-tile 26_12_2_1 at a 2 metre resolution. . . . .	23
3.5	Screenshot from input parameters used for GRASS <code>r.fillnulls</code> . . . . .	24

3.6	Graphical model for deriving seed points, which later serve as an input for seeded region growing. The model takes elevation data as input, calculates slope and surface curvatures, and reprojects the layers to the project CRS. Finally, the cells meeting a certain criterion are extracted and sieved. . . . .	25
4.1	ArcticDEM subset of sub-tile 26_12_2_1 and esker ridge lines mapped by Storrar, Stokes, and D. J. Evans (2013). Notable area 1 depicts a region where a ridge was not identified as an esker by the reference data set by Storrar, Stokes, and D. J. Evans (2013), notable area 2 displays an area with nodata values for elevation. . . . .	29
4.2	Raw seed points and seed points after sieving for exemplary region. . . . .	31
4.3	SRG based on different input parameters for exemplary region. . . . .	32
4.4	SRG with combined parameters (slope, vertical and horizontal distance, profile curvature), versus combined and thinned SRG for exemplary region. . . . .	32
4.5	3D-view of regions from SRG, with superimposed seed points and esker ridge lines from Storrar, Stokes, and D. J. Evans (2013). Vertical scale inflated by factor 2. . . . .	33
4.6	3D-view of a convex landform incorrectly detected as an esker at the edge of a former nodata field in <i>Notable Area 2</i> from fig. 4.1. Vertical scale inflated by factor 2. . . . .	34
5.1	Transect through exemplary esker, using the profile tool plug-in in QGIS. The x-axis represent metres in horizontal distance, while the y-axis represent values for different morphometric parameters based on 2 <sup>nd</sup> -order derivatives. . . . .	36
5.2	The figure is an illustration of table 4.1, displaying the three tested calculation methods by I. S. Evans (1979), Zevenbergen and Thorne (1987), and Florinsky (2009). The y-axis displays the ratio between mapped regions that are intersected by esker ridge lines of the reference data set by Storrar, Stokes, and D. J. Evans (2013) and the total area of mapped regions within the subset presented in fig. 4.1. The x-axis displays the ratio of esker ridge length mapped in the reference data set by Storrar, Stokes, and D. J. Evans (2013) that was intersected by my mapped regions versus the total length of esker ridge lines from the reference data set. The values apply to the extent displayed in fig. 4.1. . . . .	37
5.3	Transect through subjective artifact in elevation data in southern part of ArcticDEM sub-tile 26_12_2_1, using the profile tool plug-in in QGIS. Axis values in metres. . . . .	40



# List of Tables

2.1	The <i>glacier family</i> showing the classification scheme for glacier morphologies. Partially copied from D. J. A. Evans (2018). . . . .	4
2.2	Dictionaries used in this thesis. . . . .	12
2.3	Definitions from EPLa and USDA. . . . .	13
3.1	Overview of file sizes at different resolutions for tile 26_12 and sub-tile 26_12_2_1, respectively. . . . .	21
4.1	Outcome of seeded region growing based on three different calculation methods within SAGA's <b>Slope, Aspect, Curvature</b> algorithm. Numbers in subscript depict the threshold value used for seed point sieving. The total length of all eskers mapped by Storrar, Stokes, and D. J. Evans (2013) amounts to 15.61 kilometres, the total area of the subset used for the analysis in this table is equal to 101.06 square kilometres. . . . .	30
A.1	Overview of data sets used in the context of this thesis and their respective source.s . . . . .	44
A.2	Overview of software packages and libraries used in the context of this thesis. . . . .	44
A.3	Overview of dictionaries used in the context of this thesis. . . . .	45

# Introduction

The ArcticDEM provides a powerful new data source for various research areas. It is a comprehensive, high-resolution elevation model of the Arctic which was released between September 2016 and September 2018. Applications can be found in geophysics (Dai and Howat 2017; Dai, Durand, et al. 2018), forestry (Puliti et al. 2020), remote sensing (Meddens et al. 2018), or glaciology and geomorphology (Lewington, Livingstone, Sole, et al. 2019; Lewington, Livingstone, Clark, et al. 2020). It is my goal to present a new opportunity for geomorphological and glaciological research to apply this high-resolution digital land surface model. To be more precise, the thesis aims to detect and map eskers in Canada in an automated process.

## 1.1 Motivation

Eskers are a typical landform in exposed beds of paleo-ice sheets and glaciers that can be described as *elongate, straight-to-sinuuous ridges of glaciofluvial sand and gravel* (Storrar, Stokes, and D. J. Evans 2014b, p.1). Moreover, eskers record deposition in predominantly subglacial tunnel systems, but are also linked to englacial and supraglacial drainage channels. Thus, they serve as a means to reconstruct ancient glacier drainage systems. This is especially convenient as studying contemporary sub-ice sheet meltwater drainage systems is only possible through indirect methods, i.e. borehole and tracer studies, ice dynamic proxies and remote sensing (Lewington, Livingstone, Sole, et al. 2019). Oftentimes these indirect methods are costly, limited by their temporal or spatial resolution, or difficult to assess when it comes to numerical modelling (Storrar, Stokes, and D. J. Evans 2014a; Storrar, Stokes, and D. J. Evans 2014b). Exposed beds of paleo-ice sheets, however, provide an abundant and accessible repository for the reconstruction of former subglacial water flow direction, sediment flux, the position of the ice margin and ice sheets surface slope (Lewington, Livingstone, Sole, et al. 2019). Insights on said meltwater drainage systems contribute to a better understanding of glacier dynamics and movement which is crucial for glacier modelling, especially in times of rising

temperatures. While there are maps on the pattern and distribution of eskers (i.e. glaciological mapping of Canada by V. Prest, Grant, and Rampton (1968), Aylsworth and Shilts (1989), Fulton (1995), Storrar, Stokes, and D. J. Evans (2013)), the generation of these maps is based on manual mapping of remote sensing imagery, which is slow and subjective.

With the increased availability of high quality elevation data, methods for semi-automatic extraction of landforms, such as eskers (Broscoe et al. 2011), landforms associated with eskers (Lewington, Livingstone, Sole, et al. 2019), drumlins (Jorge and Brennand 2017) or valleys (Straumann and Purves 2008) were presented in scientific literature. These methods, which make use of principles of geomorphology and geomorphometry (Tomislav Hengl and Hannes I Reuter 2009), can be coupled with elevation data from ArcticDEM.

## 1.2 Research Questions & Goals

This thesis addresses the following research questions. To answer them, I first collect and present relevant literature in chapter 2. In chapter 3 I explain the methodology used to address the research questions. The results described and illustrated in chapter 4 are discussed in chapter 5.

- RQ1: Is it possible to extract eskers from the ArcticDEM in an automated process for a small study area (2500 square kilometres) in Canada?
- RQ2: How well does the automated esker-detection process perform compared to a recent data set of Canadian eskers?
- RQ3: How well does the automated esker-detection process perform in other parts of Canada?

In short, the aim of this thesis is to find a way to automatically generate an accurate distribution map of eskers based on ArcticDEM data. For this end, the work will be split into three parts. First, a landform characterisation of eskers, underlying formation processes and typical spatial properties are needed. The second objective is to find and apply methods to efficiently extract eskers differing in size and shape from the ArcticDEM. This inheres preprocessing of the data, choosing an appropriate study area and appropriate spatial algorithms and testing the methods' scalability. Finally, I propose a comparison between my own results and a reference map.

## State of Research

As the title of the thesis promises, I would like to find out how ArcticDEM can present opportunities for research. More specifically, how it can contribute to the realms of glaciology and geomorphology, and in what ways scholars have already found applications for it. This chapter lays the theoretical basis to discuss this issue by presenting the current state of the art. I first highlight aspects and concepts from glaciology and geomorphology, and introduce the ArcticDEM data set in more detail. Then, examples of existing applications and remaining research gaps are listed. Ultimately, these research gaps legitimise the purpose of the thesis and simultaneously point to the research questions stated in section 1.2.

### 2.1 Glaciology

Glaciology is the scientific discipline concerned with *all aspects of ice on landmasses. It deals with the structure and properties of glacier ice, its formation and distribution, the dynamics of ice flow, and the interactions of ice accumulation with climate* (Britannica Encyclopedia 2008). Similar to D. J. A. Evans (2018), I start by introducing the glacier family, which is a framework to display the variety of glacier morphologies in regards to their spatial and temporal properties (see table 2.1). The classification helps to grasp the breadth of glacier bodies that exist and puts them into two different classes based on spatial extent.

It is important to apprehend the diversity of glacier ice bodies to understand how glacial processes are governed by climate and topography at differing scales. These glaciological processes in turn have an influence on the climate (positive feedback mechanisms), they permanently alter the topography and reveal interesting geomorphological features during stages of advance, stagnation and retreat.

**Table 2.1** – The *glacier family* showing the classification scheme for glacier morphologies. Partially copied from D. J. A. Evans (2018).

1 <sup>st</sup> -order classification	2 <sup>nd</sup> -order classification
<i>Ice sheet and ice cap</i> (unconstrained by topography or submerging the landscape)	<i>Ice dome</i> (multiple domes and ice dispersal centres are joined by ice divides)
<i>Glaciers constrained by topography</i>	<i>Ice stream</i> (relatively fast-flowing ice)
<i>Ice shelves</i> (floating ice masses fed either by outlet glaciers and/or sea ice growth)	<i>Ice field</i> (no dome and pierced by nunataks)
	<i>Valley glacier</i> (confined by a valley, common form e.g. in the Alps)

### 2.1.1 Laurentide Ice Sheet (LIS)

The glacial ice body important to this work is the Laurentide Ice Sheet that occupied much of northern North America during the Wisconsin Glacial Stage. This epoch refers to the last glacial period between 100 and 10.5 thousand years before present and is better known as the Weichselian Stage in Europe or Würm Stage in the Alpine region. The LIS was centered over Hudson Bay and can be divided into three main sectors of ice inception. These sectors can be further subdivided into their major ice flow components (simply termed *Ice*) separated by so-called ice divides. The LIS is a system of the following sectors and their correspondent dynamically distinct components: Plains Ice and Keewatin Ice composed the Keewatin Sector, Hudson Ice and Labrador Ice composed the Labrador Sector and Foxe, Amadjuak, and Penny Ice composed the Baffin Sector (Fulton and Victor K Prest (1987)). At its greatest advance, the LIS covered an area of  $11 \times 10^6$  km<sup>2</sup> with a maximum thickness of 3 kilometres, which amounts to a sea-level equivalent (SLE) of approximately 40-50 metres (Fulton (1995)). To the east, the LIS was bounded by the Rocky Mountains, behind which stretched the Cordilleran Ice Sheet (CIS). To get a better idea of the extent of the LIS, please see fig. 2.1. For those interested, a map series by Dyke and V. K. Prest (1987) displaying the historical ice retreat outline of the LIS quite nicely.

### 2.1.2 Subglacial Meltwater Drainage Systems

Glaciers form the landscape by erosion, deposition and deformation. Much like a constantly shuffling conveyor belt D. J. A. Evans (2018), the processes of glacial erosion produce material in varying grain sizes, which is transported and later deposited. All the processes are manifested in typical features of glacial landscapes, i.e. U-valleys, moraines, drumlins or erratic boulders. Thereby both water in its frozen form and in its liquid aggregate state are fundamental to glacial processes and dynamics. Here, I will not explain ice dynamics as such, but rather focus on subglacial meltwater drainage systems and their significance for glacial dynamics.

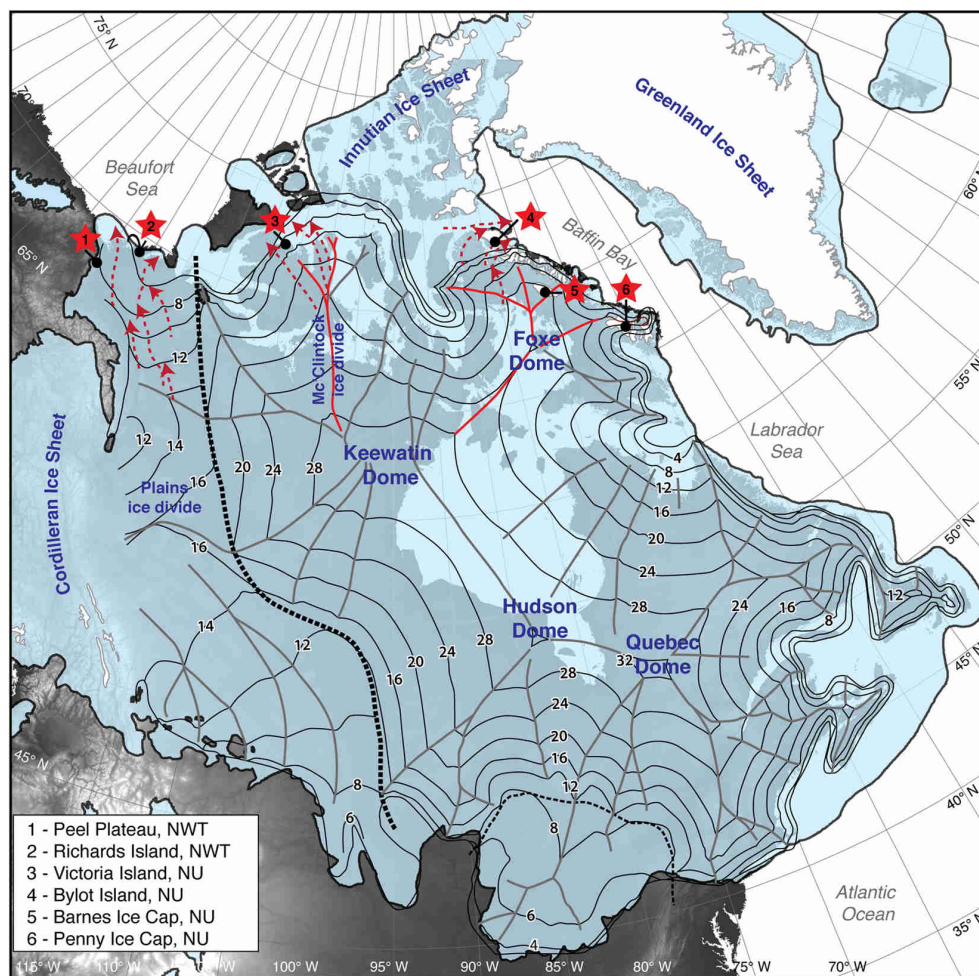


**Figure 2.1** – Extent of LIS during last glacial maximum, including reconstructed elevation. Elevation values are given in 100's of meters above present-day sea-level. The extent of the LIS (including ice-shelves) at last glacial maximum is derived from Dyke and V. K. Prest (1987). Image and data copied from Lacelle et al. (2018).

The flow of water within a glacier is driven by melting of ice due to three main heat sources. There is melt due to solar radiation (supraglacial melt), melt due to geothermal heat (subglacial melt) and melt due to glacier flow causing frictional heat at the glacier bed (subglacial melt). Glacier melt is generally seasonal as discharge and volume of meltwater increases during the ablation season. Supraglacial meltwater finds its way into the glacier and finally to the glacier bed through crevasses and moulins. There, meltwater is stored in subglacial lakes or is transported to the glacier snout by a subglacial drainage network. As the melt season progresses the englacial and subglacial drainage network develops through channel enlargement and increased connectivity, thus becoming more efficient (D. J. A. Evans (2018)). There is a differentiation between large channels that become excavated into the bedrock (N-channels, after Nye (1965)) and those that are excavated upwards into the ice (R-channels, after Röthlisberger (1972) and Shreve (1972)). Inside those subglacial channels, and with decreasing discharge and flow velocity of meltwater, sedimentation of glacial debris takes

place. For R-channels (channels excavated upwards into the ice) and englacial drainage channels, this results in stratified depositions of glacial debris. Please see fig. 2.2 for clarification. The Hooke channels visualised in fig. 2.2 are in fact R-channels that form between two melt seasons. Lewington, Livingstone, Clark, et al. (2020) and Storrar, Jones, et al. (2021) discuss the process model explaining the influence of conduit pressure on the geomorphic signature of the channels, i.e. the broadening and narrowing of R-channels.

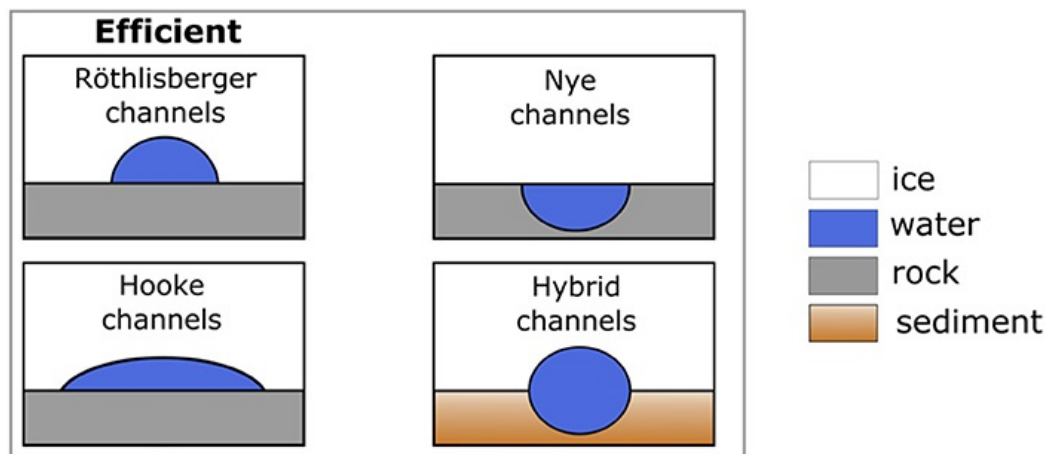


**Figure 2.2** – Simplified cross-sections of efficient subglacial drainage channels. Adapted from Davison et al. (2019).

## 2.2 Geomorphometry

Geomorphometry can be described as *the science of quantitative land-surface analysis* (Pike, I. Evans, and T. Hengl (2009)). It emerged from geo-sciences, mathematics and computer science and is applied in various other scientific fields such as civil engineering, military engineering, space exploration and more. Although its roots most certainly lie with the ancient Egyptians and the ancient Greeks, geomorphometry as we understand it today evolved in the 19th century by quantifying the Earth’s surface and classifying its morphology (Gauss (1828), Maxwell (1870), and Penck (1894)). With the advent of computers, the research field developed more rapidly as calculation of spatial algorithms became greatly facilitated and more efficient. Today, geomorphometry is concerned with the description and processing of elevation data, and its visualisation. It focuses on discrete land-surface features (*specific geomorphometry*) and the continuous land surface as such (*general geomorphometry*), but covers the entire spectrum between those two concepts (see fig. 2.3). The fundamental operation in geomorphometry is taking a digital representation of the land surface (i.e. digital land surface model DLSM) and extracting objects and measurements from it. As advised by Pike, I. Evans, and T. Hengl (2009), I will use the term *geomorphometry* to refer to the scientific discipline of topographic quantification. Furthermore, *land surface* denotes geomorphometry’s study focus, using a digital rep-

resentation of the land surface as input. The two terms *digital land surface model DLSM* and *digital elevation model DEM* are treated equally. The *digital surface model DSM* is a specific type of surface model, e.g. a canopy height model or a surface model showing slope gradient or higher derivatives of elevation.

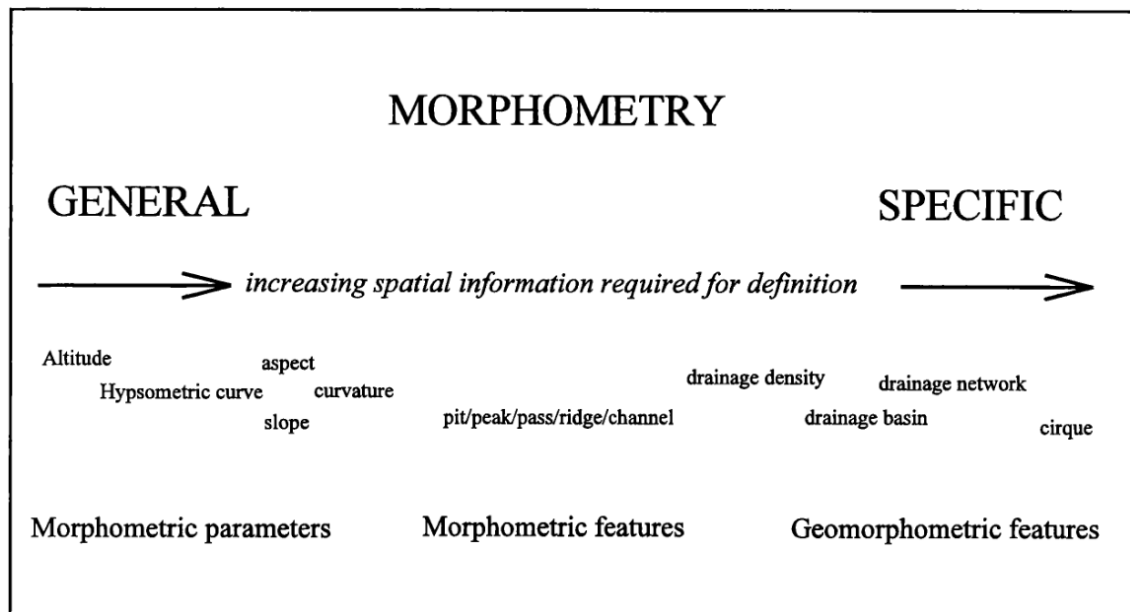


**Figure 2.3** – The spectrum between general and specific geomorphometry, copied from Wood (1996).

Usually, the workflow in geomorphometry includes one or all of the five following steps:

1. Surface sampling: Sampling of the Earth's surface with the help of remote sensing techniques or in-situ methods.
2. Surface generation: Generating a surface model from the sampled elevation points, most likely resulting in a *triangulated irregular network* (TIN) of the sampled heights.
3. Preprocessing: Errors and artefacts are being removed and corrected (see section 3.2.3 for the preprocessing performed in this thesis, for more information refer to H. I. Reuter et al. (2009)).
4. Surface analysis: Deduce objects and land-surface parameters from elevation data (see section 3.2)
5. Application: Usage of deduced objects and parameters for desired issue.

### 2.2.1 Basic Land-Surface Parameters

Slope, aspect and curvature, catchment area and visibility are examples for geomorphometric parameters (LSP). Moreover, they are basic land-surface parameters, as they can be derived directly from



a DEM ignoring related formational processes and without knowledge of the area focused on. Only geometrical and topological characteristics of the DEM are analysed which is simple, but useful for many applications. LSP can be divided into two groups based on the focus chosen for calculation. Local LSP (e.g. slope, aspect and curvature) are derived locally, around the morphometry of one cell and usually computed within a moving  $3 \times 3$  neighbourhood. Of course, search windows with larger edge lengths or circular foci are possible, too. Regional LSP on the other hand take larger parts or even the whole DEM as input for analysis. A classic example for regional LSPs is the creation of catchment areas or performing a visibility analysis. I will primarily focus on explaining local LSPs, as they are more relevant to this thesis. Local LSPs utilize concepts from differential geometry to derive measures such as slope, aspect or different surface curvatures. Moreover, statistical key figures provide parameters about range and standard deviation in the elevation data, terrain roughness or anisotropy (Olaya (2009)). In the following, I explain not all, but most of these parameters and their derivation.

### 1<sup>st</sup> Order Derivatives of Elevation Data: Slope and Aspect

Finding the maximum rate of change of elevation in two dimensions (i.e.  $x$  and  $y$  direction) can be used to identify the gradient (I. S. Evans (1972), Wood (1996), and Olaya (2009)). A surface can be approximated using a bivariate quadratic function according to the original Evans method:

$$z = ax^2 + by^2 - cxy + dx + ey + f \quad (2.1)$$

where the two partial derivatives for both dimensions  $x$  and  $y$  are given as

$$\frac{\delta z}{\delta x} = 2ax + cy + d, \quad \frac{\delta z}{\delta y} = 2by + cx + e. \quad (2.2)$$

Consequently, the gradient is expressed as

$$\nabla \bar{Z} = \left( \frac{\delta z}{\delta x}, \frac{\delta z}{\delta y} \right), \quad (2.3)$$

from which slope gradient and aspect can be derived. Since we want to calculate slope and aspect at the central point of the quadratic surface (i.e. central cell of the analysis window), applying a local coordinate system with its origin at the central cell leaves us with  $x = y = 0$ , giving:

$$d = \frac{\delta z}{\delta x} = \frac{z_3 + z_6 + z_9 - z_1 - z_4 - z_7}{6 \cdot \Delta s} \quad (2.4)$$

$$e = \frac{\delta z}{\delta y} = \frac{z_1 + z_2 + z_3 - z_7 - z_8 - z_9}{6 \cdot \Delta s} \quad (2.5)$$

Finally the unique values for slope and aspect can be obtained:

$$SLOPE = \arctan(\sqrt{d^2 + e^2}) \quad (2.6)$$

$$ASPECT = 180 - \arctan\left(\frac{d}{e}\right) + 90 \cdot \frac{e}{|e|} \quad (2.7)$$

Regarding the aspect, the direction of origin of the coordinate system is important. For eq. (2.7), the measures are given in degrees, read clockwise from north, ranging from  $0^\circ$  to  $360^\circ$  (Gallant and Wilson (1996)). Furthermore, aspect cannot be defined where the gradient equals zero, which makes sense from a mathematical as well as a topographical point of view.

## 2<sup>nd</sup> Order Derivatives of Elevation Data: Curvatures

Involving second order derivatives allows statements regarding the concavity and convexity of the surface. The parameter describing this is called curvature. However, a point on a surface exhibits different curvature values depending on the orientation of the intersecting plane with the normal section of the surface (Wood (1996) and Olaya (2009)). There are four simple directions on a smooth surface to select from fig. 2.4.

*P.A. Shary et al. / Geoderma 107 (2002) 1–32*

17

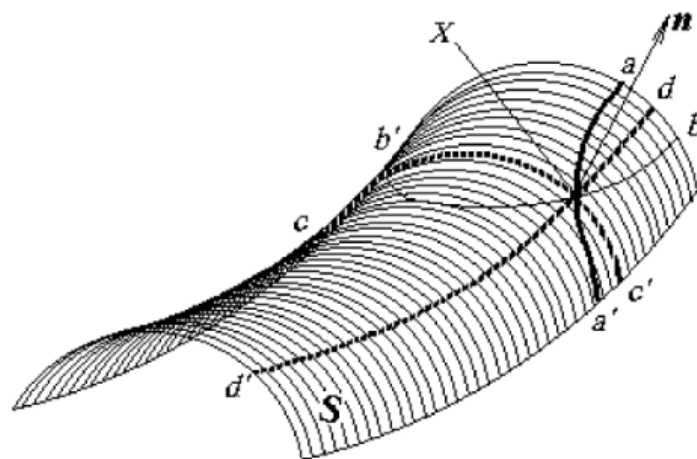


Fig. 6. The four directions naturally marked on the surface  $S$ .  $n$ —normal vector to  $S$  at the point  $X$ ;  $aa'$ —gradient line;  $bb'$ —contour line;  $dd'$ ,  $cc'$ —main normal sections.

**Figure 2.4** – curvatures, copied from Peter A. Shary, Sharaya, and Mitusov (2002)

- **PROFC** or profile curvature: Intersecting with the plane of the Z axis and aspect direction

(that of normal section  $aa'$  in fig. 2.4, synonymous with vertical curvature).

- **TANGC** or tangential curvature: Intersecting with the X Y plane (that of normal section  $bb'$  in fig. 2.4, synonymous with plan curvature or horizontal curvature).
- **MAXC** or maximum curvature: Plane of maximum curvature (that of normal section  $cc'$  in fig. 2.4).
- **MINC** or minimum curvature: Plane of minimum curvature (that of normal section  $dd'$  in fig. 2.4).
- **LONGC** or longitudinal curvature: Intersecting with the plane of the slope normal and aspect direction.

PROFC and TANGC are physically demarcated by the gravitational field, meaning profile curvature runs perpendicular to contour lines while tangential curvature runs lays in the same plane as the contour line intersecting the point X in fig. 2.4

### A Statistical LSP: Terrain Ruggedness Index

One local, statistical land-surface parameter applied in this thesis is the terrain ruggedness index (TRI) by Riley and Degloria (1999). The measure represents the mean change in elevation between a grid cell and its neighbours. Originally, the calculation in Riley and Degloria (1999) was bound to a  $3 \times 3$  analysis window. In the algorithm provided by GDAL (please see section 3.2.3 or appendix A) used for my workflow, this calculation is altered by taking the mean of the absolute deviations. Olaya (2009) points out the crucial role of the size of the analysis window as well as the grid resolution.

#### 2.2.2 Landforms

Following the definition by MacMillan and P. A. Shary (2009), a landform is a *physical feature of the Earth's surface having a characteristic, recognisable shape and produced by natural causes*. They can be described either based only on geometric properties (Gauss (1828)) or based on subjective conceptual mental models expressed by semantics (Dehn, Gärtner, and Dikau (2001) and Straumann and Purves (2008)). Furthermore, most classifications of landforms consider how the gravitational field and thus gravitational processes interact with the land surface. Therefore, understanding the processes that influenced or will influence a landform's shape, size, or contextual position and orientation is essential for classification and extraction of landforms. Features that are considered a landform are plains and mountains, ridge lines, slope lines, or special points like peaks, passes and pits. In glacial geomorphology, examples may include drumlins, moraines, megascale glacial lineations, and eskers (I. S. Evans (2012)). It is important to mention that the choice of scale plays a key role in detecting or even perceiving different landforms. Landform classification are commonly specific to a

particular scale or a small range of scales. Most commonly this happens on a micro (1 metres - 100 metres) and meso (100 metres - 10 kilometres) terrain extent according to Dikau (1990).

Landforms can be classified into elements (i.e. landform elements). They are considered portions of a landform with relatively similar shape, steepness, orientation or relative position (MacMillan and P. A. Shary (2009)). To illustrate this concept, I include fig. 2.5 showing the 10 most common landform elements according to Jasiewicz and Stepinski (2013). An extensive list of framework classifying landform elements can be found in MacMillan and P. A. Shary (2009)).

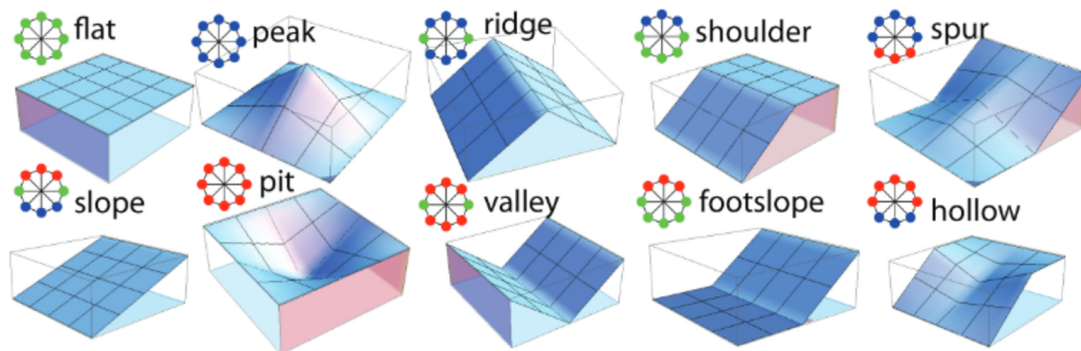


Figure 3: Symbolic 3D morphologies and their corresponding geomorphons (ternary patterns) for the 10 most common landform elements.

**Figure 2.5** – Geomorphons for the ten most common landform elements and their 3D- representation in the form of morphometric feature types. Copied from Jasiewicz and Stepinski (2013)

A method of automated extraction of geomorphometrical entities is generally based on selecting rules for a set of input variables with which a relationship with expected output in form of landforms or landform elements is predicted. A crucial milestone in any method to automated landform classification is thus to gain domain knowledge of the landform of interest. This knowledge may be in written form as well, but must be put into digital parameters eventually to obtain a set of suitable input variables (MacMillan and P. A. Shary (2009)). MacMillan and P. A. Shary (2009) propose a modification of the three step workflow described by Weibel and DeLotto (1988):

- Establishment of the spatial object(s) of classification;
- Specification and computation of the input variables;
- Extraction or creation of the classification rules;
- Application of the classification rules;
- Evaluation and assessment of accuracy.

### 2.2.3 Eskers: Extracting Domain Knowledge about a Landform

As learned above, the first activity in the process of automated landform extraction is to establish the spatial object of classification. Similar to Straumann (2010), I will start from existing corpora of descriptions in order to elucidate the landform that I want to extract: eskers. Eskers are also referred to as eskar, eschar, os, asar or osar. Henceforth, only the term esker will be used to prevent confusion among terms that are considered synonyms. Scholars before me have studied the breadth of landforms and structured them into taxonomies. These taxonomies can be employed to find esker characteristics, as well as terms for superordinate landforms and their geometric properties. Knowledge about landforms hierarchical to the landform of interest allows for a more bottom-up conceptualisation. Also landform elements typical to eskers can be identified through this step. The sources of classifications are derived from dictionaries or feature sections of data exchange standards and are shown in table 2.2. Supplementary to eskers, the landform element ridge is described below, with a definition from EPLa and USDA shown in table 2.3. Further below I embed the term ridge in a more geomorphometric context, where it is introduced as one of the six morphometric feature types defined by Wood (1996).

**Table 2.2** – Dictionaries used in this thesis.

Name	Abbreviation
Encyclopedia of Planetary Landforms	EPLa
Oxford Dictionary of Geography	ODGeo
United States Dept. of Agriculture: Natural Resource Conservation Service	USDA

A ridge is one of the six morphometric feature types as defined by Wood (1996). Besides ridge, a point on a surface can be attributed to one of the following morphometric feature types, as illustrated in fig. 2.6: Channel, pass, peak, pit and plane. This attribution is based on a combination of second order derivatives of the surface and within a given neighbourhood around the point. For raster data, usually a quadratic search window consisting of  $3 \times 3$  or  $5 \times 5$  cells is selected for this purpose. If the center cell of the search window *lies on a local convexity that is orthogonal to a line with no convexity / concavity* (Wood (1996)) it is considered part of a ridge. Figure 2.6b illustrates the situation: Cell 5 is the center of the search window in a  $3 \times 3$  neighbourhood. Cells 1, 4, 7 and cells 3, 6, 9 turn cell 5 into a local convexity (*lies on a local convexity*), while cell 2 and 8 are on the same height (*a line with no convexity / concavity*).

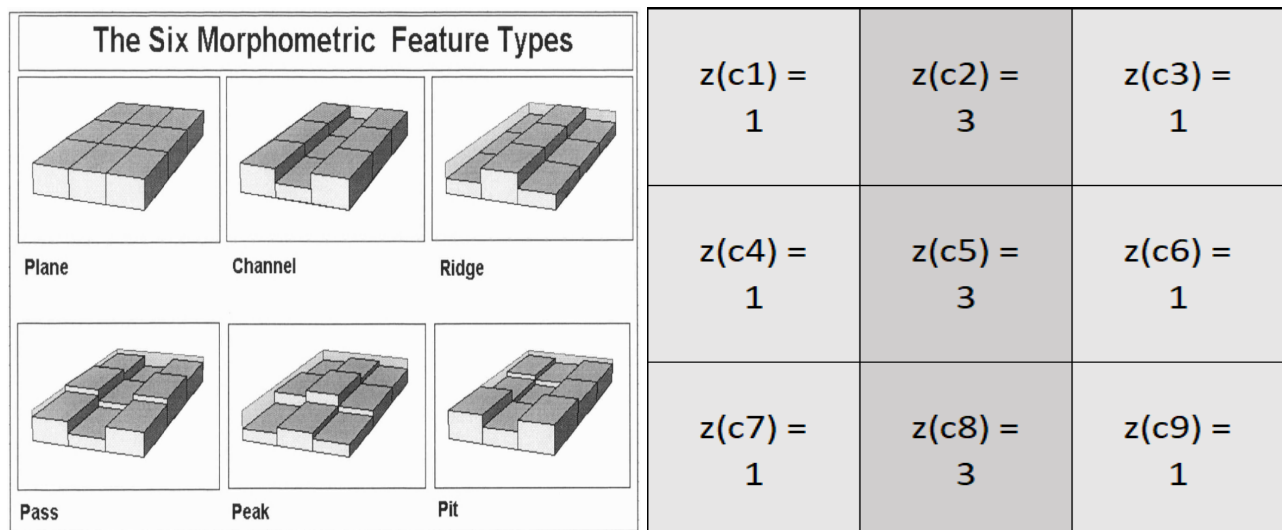
$$\frac{\partial^2 z}{\partial x^2} > 0, \quad \frac{\partial^2 z}{\partial y^2} = 0 \quad (2.8)$$

**Table 2.3** – Definitions from EPLa and USDA.

Landform (Element)	Source	Definition
Esker	EPLa	Straight-to-sinuuous ridge composed of sand/gravel, deposited in a confined glacial meltwater drainage channel. Winding, steep sided, narrow, sharp- to broad-crested ridges of cross-stratified and massive sand, gravel, and boulders. May be mistaken for other slightly sinuous or linear ridge types. In planform, eskers can be sinuous, anastomosing, and/or discontinuous. Isolated, closed depressions (kettles), commonly water filled, may flank or be part of broader esker ridges.
	ODGeo	A long ridge of material deposited from meltwater streams running subglacially, roughly parallel to the direction of ice flow, and ranging from tens of metres to several hundred kilometres, as in Finland. Eskers wind up and down hill because subglacial streams are under great hydrostatic pressure, and can flow uphill. Brennan (2002) <i>Geomorph.</i> 32, 3–4 identifies and investigates five types of esker. Thomas and Montague (1997) <i>Quat. Sci. Rev.</i> 16 argue that glacial lake systems are crucial for the development of esker systems.
	USDA	A long, narrow, sinuous and steep-sided ridge composed of irregularly stratified sand and gravel deposited as the bed of a stream flowing in an ice tunnel within or below the ice (subglacial) or between ice walls on top of the ice of a wasting glacier, and left behind as high ground when the ice melted. Eskers range in length from less than a kilometer to more than 160 kilometers, and in height from 3 to 30 meters.
Ridge	EPLa	Positive relief feature of varying origin.
	USDA	A long, narrow elevation of the land surface, usually sharp crested with steep sides and forming an extended upland between valleys. The term is used in areas of both hill and mountain relief.

## 2.3 Seeded Region Growing

Seeded region growing or simply region growing is a class of image segmentation techniques. The starting point are single pixels, so-called seed points. Based on these seeds, surrounding pixels are added if they fulfil a certain similarity criterion. This similarity criterion is a chosen threshold or a set of thresholds considering radiometric or spatial distance (Bechtel, Ringeler, and Böhner (2008)). The clusters of newly added pixels and their respective seeds points are called regions, thus region growing. There are different approaches to this technique, e.g. Basic Region Growing or Segmenatation via Brownian motion (Erikson (2004), Erikson (2003), and Erikson and Olofsson (2005)). Moreover, SAGA GIS provides an algorithm that allows to manually add defined seed points. Then, based on defined thresholds in position space (i.e. distance from seed points given as maximum number of cells) and feature space (distance from seed points considering a certain attribute, e.g. spectral



(a) *The Six Morphometric Feature Types* as in Wood (1996, p. 112): Plane, Channel, Ridge, Pass, Peak and Pit. (b) Representation of a ridge in a grid in  $3 \times 3$  window, own representation.

**Figure 2.6** – Classification of morphometric feature type and conceptual illustration of a ridge in a grid.

reflectance, slope, change in curvature) unclassified pixels are merged with the existing region.

## 2.4 ArcticDEM

This section introduces the ArcticDEM as a DLSM in raster format and as this thesis's main data set. In one sentence, the ArcticDEM is an *NGA-NSF public-private initiative to automatically produce a high-resolution, high quality, digital surface model (DSM) of the Arctic using optical stereo imagery, high-performance computing, and open source photogrammetry software* (Porter et al. (2018)). In other words, ArcticDEM is a the National Geospatial-Intelligence Agency (NGA) and the National Science Foundation (NSF) joint-research project to produce a DSM of the Arctic in a 2m spatial resolution. It covers all land area north of 60° North including all territory of Greenland, the entire state of Alaska, and the Kamchatka Peninsula of the Russian Federation. The data set was released in batches between September 2016 and September 2018, covering  $23 \times 10^6$  km<sup>2</sup> land area in its current state. As data basis, DigitalGlobe's WorldView-1, WorldView-2, and WorldView-3 satellite constellation collected stereoscopic high-resolution imagery (0.5m) of the Arctic. A small portion of data was also generated from the GeoEye-1 satellite sensor. This surface data consisting of stereopair images was then processed to a DLSM using Surface Extraction from TIN-based Searchspace Minimization (SETSM, *SETSM by MJ Remote Sensing* (n.d.)) software. The ArcticDEM is projected to WGS 84 / NSIDC Sea Ice Polar Stereographic North (EPSG:3413) publicly available in 2m, 10m, 32m, 100m, 500m and 1km resolution. Laser altimetry data from the NASA IceSAT spacecraft has been applied to the ArcticDEM mosaic tiles in order to increase absolute accuracy of the data. The ArcticDEM strips, however, come without the correction, which leaves them with an absolute accuracy is approx-

imately 4 meters in horizontal and vertical planes. This is one of the reasons why mosaic files are used in this thesis. Another argument for using mosaic files: They are compiled from the best quality strip DEM files to reduce void areas and edge-matching artifacts. Still, void areas and artifacts from atmospheric obstructions occur. The ArcticDEM is not a *bare earth* product, meaning that source imagery from satellites cannot penetrate vegetation or man-made objects (Porter et al. 2018).

### Recent Applications with ArcticDEM

As mentioned in chapter 1, the ArcticDEM has already found use in research. Applications include work on elevation change of lava flows on Kamchatka (Dai and Howat 2017) and elevation change of shorelines in Alaska (Dai, Durand, et al. 2018), the generation of a canopy height model for a small study area in Alaska (Meddens et al. 2018), and modelling of above-ground biomass stock in Norway (Puliti et al. 2020). A recent application in glaciology and geomorphology utilizing the ArcticDEM data set is published by Lewington, Livingstone, Sole, et al. (2019) where they map the outline of so-called hummock corridors in Canada and northern Scandinavia. Hummock corridors are elongated subglacial meltwater corridors, usually located around eskers. Figure 2.7 illustrates the size of mentioned hummock corridors and their spatial alignment in regards to eskers.



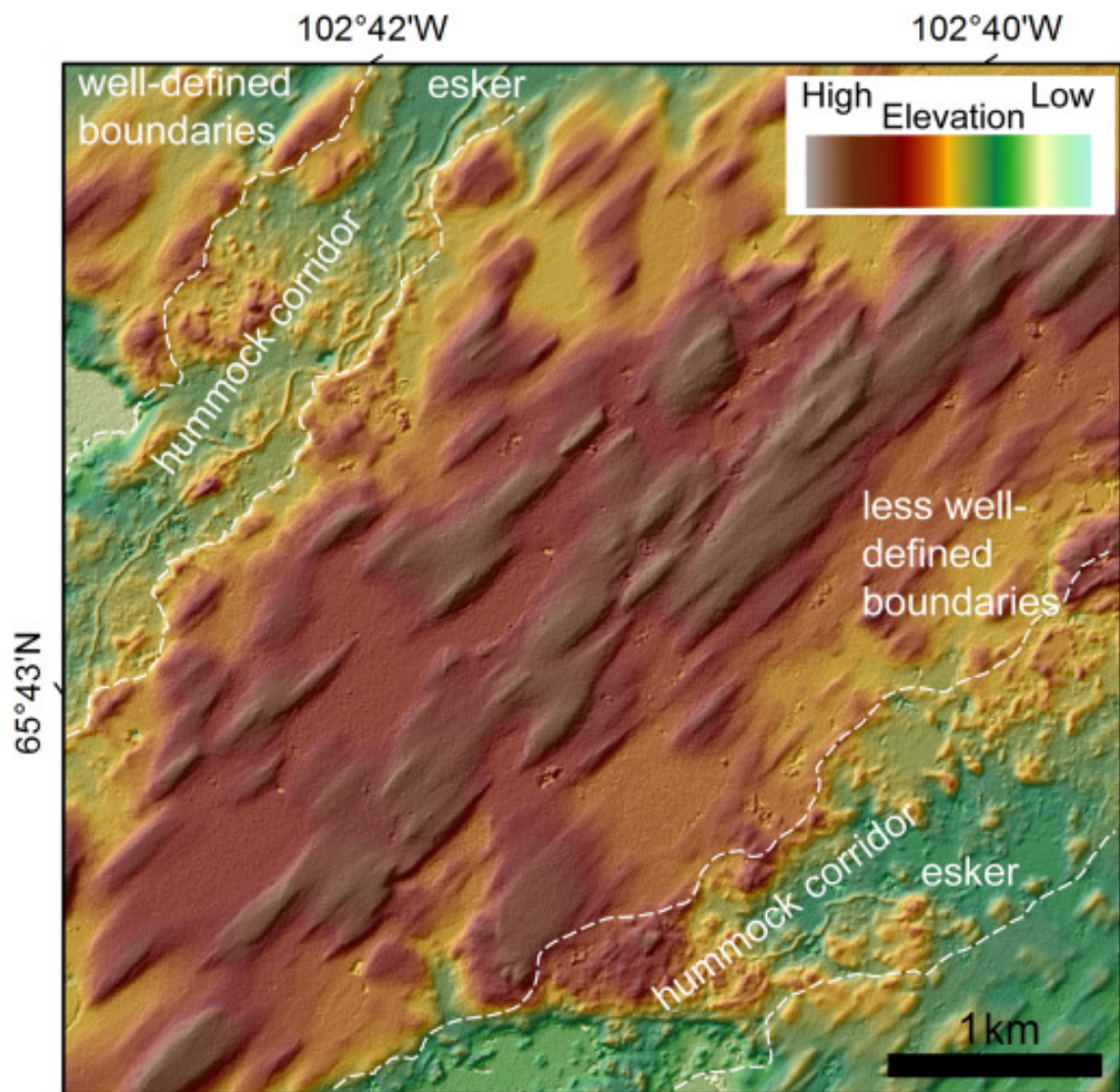


**Figure 2.7** – Eskers accompanied by elongated hummock corridors. Copied from Lewington, Livingstone, Sole, et al. (2019).

## Data and Methods

In the last chapter I discussed concepts and knowledge relevant to the topic. The following section introduces the data utilized in the course of this thesis and explains why those data sets were chosen. This is followed by an introduction of the employed software and a detailed methods section.

### 3.1 Data

I mainly used two different data sources. On one hand, there is the elevation data from ArcticDEM in a raster data format. On the other hand, I chose a shapefile containing eskers mapped by Storrar, Stokes, and D. J. Evans (2013), conveniently stored as line features. Furthermore, geological maps of Canada were consulted to obtain a qualitative feeling of geological prerequisites for esker deposition. An overview of all data sets can be found in appendix A.

#### 3.1.1 ArcticDEM: Elevation Data

The data set holding elevation information needed for the geomorphometrical analysis is the ArcticDEM. As mentioned in section 2.4, ArcticDEM is a high-resolution digital surface model of the Arctic. It covers all landmass north of 60° North plus the State of Alaska, the Kamchatka Peninsula and Greenland (section 3.1.1). For its creation optical stereo imagery and an open source photogrammetry software was deployed (*SETSM by MJ Remote Sensing* (n.d.). Porter et al. (2018)). Initially it needs to be mentioned that ArcticDEM is a digital surface model. Meaning it does not depict Earth's bare surface but rather Earth's surface with all its objects on in. This is not ideal for geomorphological mapping, since I am interested in terrain without objects such as trees or houses or snow cover. However, this fact is ignored for the most part, as there are bigger artefacts in the data itself, which will be addressed later. Furthermore, settlements are not expected in the study area and would leave a pattern in the outcome that could rather easily be detected.

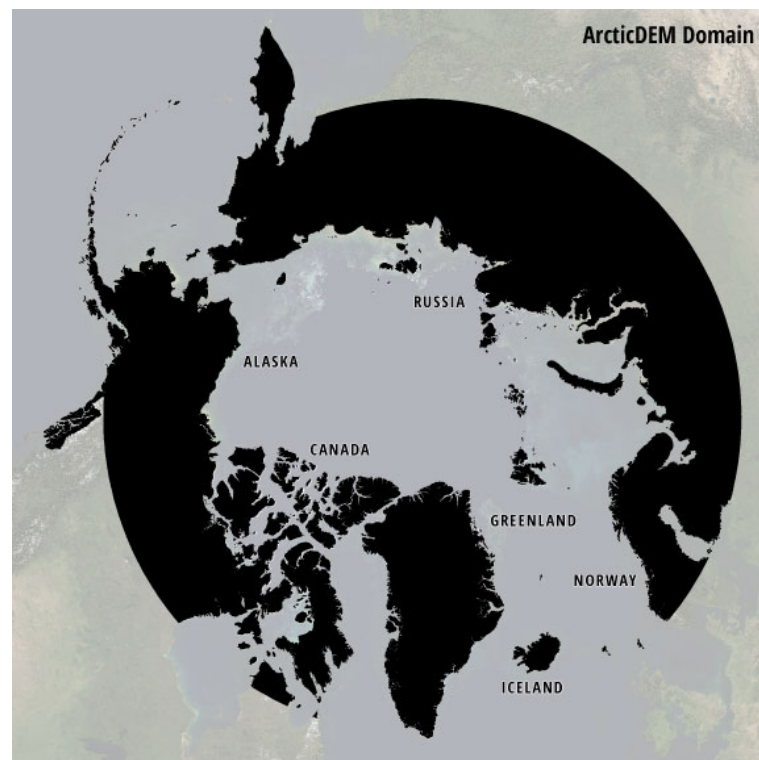


**Figure 3.1** – Domain of ArcticDEM, covering all landmass above 60° North, as well as Alaska, Greenland and the Kamchatka Peninsula in their entirety. Extent after latest and final release 7 in 2016.

The high-resolution elevation data is readily available for download at the Polar Geospatial Center (see appendix A). Here, you can choose to obtain the elevation data as strip DEM files or mosaic DEM files. Both strip and mosaic are provided in 32-bit GeoTIFF file format and come at a 2 metre spatial resolution. Elevation is given in metres, referenced to the WGS84 ellipsoid. The mosaic files, henceforth referred to as DEM tiles, are also available at reduced resolutions with cell sizes of 10 metres, 32 metres, 100 metres, 500 metres and 1 kilometre. For every file, metadata reporting RMSE in all three dimension are given.

### 3.1.2 Eskers\_Canada.shp: Reference Data on Eskers

In order to make an estimate of accuracy concerning my results, a reference data set for comparison is needed. I selected a data set holding a record of 20'186 individual eskers all deposited in Canada by the Laurentide Ice Sheet (LIS) (Storrar, Stokes, and D. J. Evans (2013)). Their ridges vary between 20 metres and 97.5 kilometres in length with a mean of 3.5 kilometres. About 9'000 eskers are situated above 60° North, most of them located around the initial position of the Keewatin ice divide, radially branching away from the center of the ice divide. Thus, 9'000 individual esker ridges lie within the extent of ArcticDEM and are relevant for the planned comparison. In their work, the mapping is based on the identification of eskers from Landsat 7 Enhanced ThematicMapper (ETM+) imagery. ETM+ has a resolution of about 30 metres (or 15 metres in the panchromatic band) and excellent spatial coverage.

In addition, there is another data set, or rather an evaluation of the map just described. Storrar, Jones, et al. (2021) surveyed their sample of large Canadian eskers, as well as eskers from Finland using 3D morphometry. The results include information on typical height, width, segment length, sinuosity and slope angle, as well as characteristic height-to-width ratio, length-to-sinuosity ratio. Out of these parameters, I will be using height, width and slope of the Canadian eskers as threshold in the calculations to come.

## 3.2 Methods

Now that we have gotten accustomed to the data, an elucidation of the planned work process is appropriate. An illustration of it can be seen in fig. 3.2. Firstly, I will explain the thought process behind the choice of study area and elaborate the necessary preprocessing steps for the input data. Secondly, esker characteristics ascertained through literature must be collected and put into measurable parameters. Then, I demonstrate an approach to detect esker ridges which is one of the milestones stated in chapter 1. These ridge lines later serve as seed points for the seeded region growing algorithm that maps the shape and outline of eskers in entirety. Finally, I present strategies for evaluation of the landform extraction method applied in this thesis.

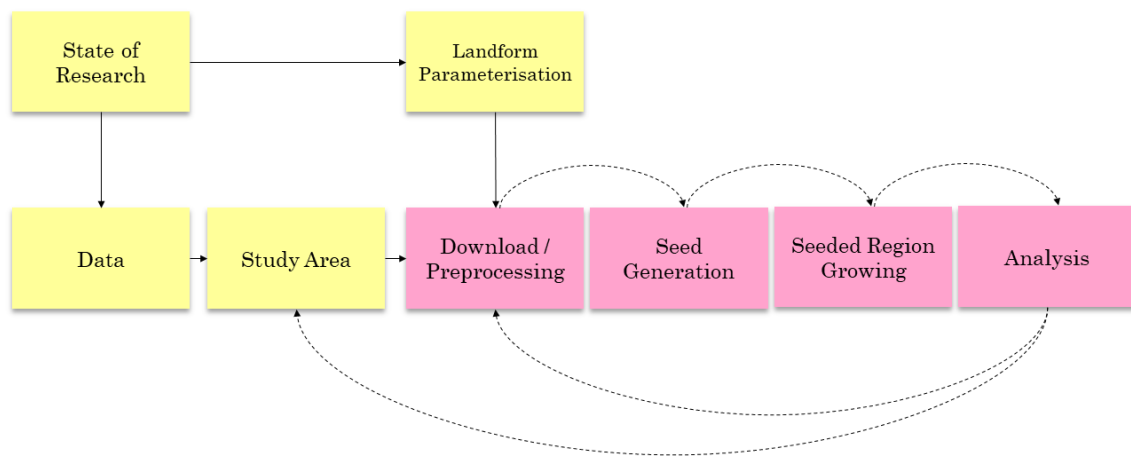


**Figure 3.2** – Planned conceptual workflow.

### 3.2.1 Software

The software used for the main part of the work at hand is to QGIS v3.16. Native to the full installation of QGIS functionalities of the following providers are included:

- Geospatial Data Abstraction Library (GDAL)
- Geographic Resources Analysis Support System (GRASS)
- System for Automated Geoscientific Analyses (SAGA)

The integration of SAGA's current distribution into to QGIS v3.16 is not fully supported during the time of writing, leading to errors during utilisation of its algorithms in to QGIS. However, this problem can be circumvented with a plugin called Processing Saga NextGen Provider. For more information on each provider and the corresponding software versions used for this thesis, please see appendix [A](#).

### 3.2.2 Study Area

Before settling for specific ArcticDEM tiles as a study area, I set the following requirements to help me find a meaningful location and size.

1. The area must be located in Canada and a latitude of over 60° North.

2. The area must be located in one of the regions more thoroughly surveyed by Storrar, Stokes, and D. J. Evans (2013), Storrar, Stokes, and D. J. Evans (2014a), and Storrar, Stokes, and D. J. Evans (2014b).
3. The area must be small enough so that the raster file does not exceed a critical size where calculation are limited by hardware and software.

Requirement (1) is a given, since an overlap between elevation data (ArcticDEM) and reference data (Map of Canadian Eskers) is necessary for a comparison. By areas *more thoroughly surveyed* by Storrar, Stokes, and D. J. Evans (2013) in requirement (2) I refer to the areas where they compared their findings based on Landsat ETM+ imagery with mapping from high resolution aerial photographs (see Storrar, Stokes, and D. J. Evans (2013), p. 459, table 1). Only two comparison areas (Dubawnt Lake Area in Nunavut and McCann Lake Area in Northwest Territory Requirement) are situated above 60° North, which narrows the search for a study area further down. Finally, requirement (3) is important for testing of ideas and concepts, as a larger study area correlates with longer calculation times and eventually software crashes. Please note the rapid change in file size at different resolutions in table 3.1.

In line with the above stated, I decided to use mosaic tile 26\_12. This tile is situated in the South-East of the Northwest Territory in Canada, with its centroid located at 61.086° North and -108.034° West. To execute investigations on the raster more efficiently, I chose subtile 26\_12\_2\_1 for a starting point. It has an interesting quantity of nodata areas, mostly due to lakes, and also shows minor cloud coverage. I want to include those regions to test the robustness of the preprocessing step explained in section 3.2.3.

**Table 3.1** – Overview of file sizes at different resolutions for tile 26\_12 and sub-tile 26\_12\_2\_1, respectively.

Tile Name	Cell Size	Tile Size	Spatial Extent
26_12_32m	32m	38 MB	100 km × 100 km
26_12_10m	10m	371 MB	100 km × 100 km
26_12_2m	2m	9 453 MB	100 km × 100 km
26_12_2_1_2m	2m	2 308 MB	50 km × 50 km

### 3.2.3 Download and Preprocessing

#### ArcticDEM mosaic batch download

ArcticDEM mosaic tiles are available from PGC at the University of Minnesota. Access is either possible via the included ESRI Web Service or PGC’s server file system. However, I decided to

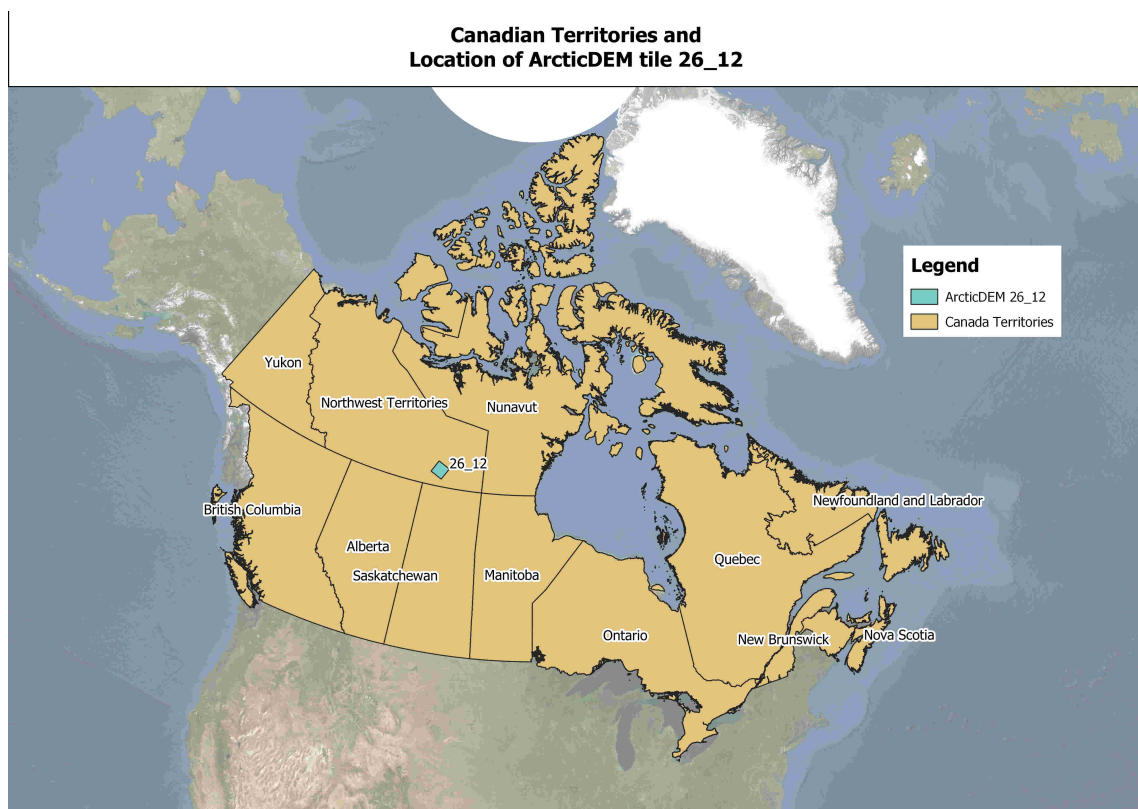


**Figure 3.3** – ArcticDEM tile 26\_12 located in the McCann Lake Area, North West Territories, Canada.

deploy a HTTP pull application for batch download (e.g. *GNU wget* or *Rstudio*). Instructions for the last two options are provided on my github (see appendix A).

### GDAL: Retile into VRT

As sub-tile 26\_12\_2\_1\_2m is still too comprehensive for the testing of different spatial algorithms I divided it into smaller squares. `gdal_retile.py` allows reallocation of the grid cells into smaller entities of equal edge length, so-called virtual raster tiles. By default, the output is labelled with the original file name and an index. I opted for an edge length of 5000 cells, which results in 25 VRTs from sub-tile 26\_12\_2\_1\_2m.

### Coordinate Reference System

The two main data sets come in different coordinate reference system. The ArcticDEM uses EPSG:3413, the reference data set for esker ridges uses ESRI:102002. I keep the ArcticDEM's coordinate reference system and reproject the esker ridge line into EPSG:3413 as well, as it assumed that it is suitable for small scale mapping in the Arctic.

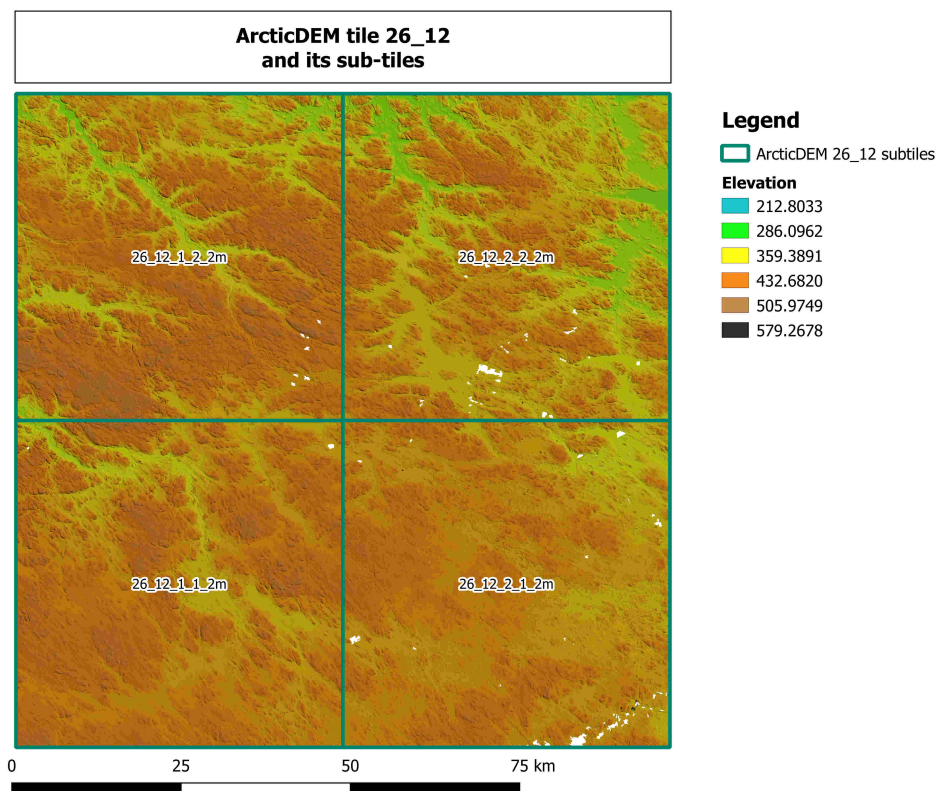


**Figure 3.4** – Division of tile 26\_12 into four sub-tiles. This work focuses on sub-tile 26\_12\_2\_1 at a 2 metre resolution.

### Fill *nodata* Areas, Atmospheric Obstruction

Even though the mosaic DEM files are a compilation of those ArcticDEM strips with the best quality (Porter et al. (2018)) there are raster patches where the z-value hold *nodata*. As the surface model is optically derived, water bodies and impact the model’s accuracy and atmospheric obstruction (e.g. clouds, fog, shadows) can result in data gaps. Filling these can be achieved both with `gdal_fillnodata.py` or by applying `grass_r.fillnulls.py`. Parameters for this step must be chosen carefully. If the search window for cells to derive values from is defined too narrowly, the patches are not being filled completely and disrupt subsequent algorithms. Too many input cells provoke overshooting. The final input parameters for the algorithm which I found effective for the study area can be seen in fig. 3.5.

Dealing with elevation data where the cell values are not NULL but are overestimated due to atmospheric obstruction is more delicate. These values are incorporated for DEM production and are not as evident as missing data in the final result. To account for that, I calculated the terrain ruggedness index and assign *nodata* to those raster cells with a TRI > 20. The new nodata areas can be interpolated similar to the process described above. The index represents the mean change in elevation between a grid cell and its neighbours, over a user-specified moving window size. The



original calculation in Riley and Degloria (1999) used only a 3x3 neighbourhood and represented the sum of the absolute deviations between the center pixel and its immediate 8 neighbours. In GDAL's `r.tri`, this calculation is modified so that the calculation can be extended over any scale by taking the mean of the absolute deviations.

The screenshot shows the input parameters for the GRASS GIS tool `r.fillnulls`. The parameters are as follows:

Parameter Name	Value
Interpolation method to use	bilinear
Spline tension parameter [optional]	40.000000
Spline smoothing parameter [optional]	0.100000
Width of hole edge used for interpolation (in cells) [optional]	3
Minimum number of points for approximation in a segment (>segmax) [optional]	600
Maximum number of points in a segment [optional]	300
Tychonov regularization parameter (affects smoothing) [optional]	1.000000

**Figure 3.5** – Screenshot from input parameters used for GRASS `r.fillnulls`

### 3.2.4 Landform Parameterisation

The term parameterisation has been described as *a set of measurements that describe topographic form well enough to distinguish topographically disparate landscapes* (Pike (1988)). In other words, the aim is to find as few terrain parameters as possible that, if combined, hold maximum information about the landform and are as globally applicable as possible (Wood (1996)). It is known from chapter section 2.2 that an esker is a *long sinuous ridge of material deposited from meltwater streams running subglacially, roughly parallel to the direction of ice flow, and ranging from tens of metres to several hundred kilometres [...]. Eskers wind up and down hill because subglacial streams are under great hydrostatic pressure, and can flow uphill* (Susan Mayhew 2015). Furthermore, Storrar, Jones, et al. (2021) provide information regarding the distribution of height, width, length and sinuosity of individual esker segments in Canada ( $n = 40'705$ ). From this they were able to derive and plot typical ratios between height and width, typical ratios between length and sinuosity and make statements about slope gradient, cross-sectional area and cross-sectional asymmetry.

### 3.2.5 Finding Ridge Lines

Finding ridge lines and, specifically finding esker ridge lines, would allow me two things. On the one hand comparison with the *Large Map of Canadian Eskers* (Storrar, Stokes, and D. J. Evans (2013)) becomes possible (section 3.2.8). On the other hand the outcome of this step are the seed points later needed for seeded region growing. Based on the knowledge from section 3.2.4, SRG allows us to approximate the shape and extent of eskers. For this end I run SAGA's module `Slope, Aspect, Curvature` fig. 3.6 on the preprocessed elevation data. This algorithm calculates slope,

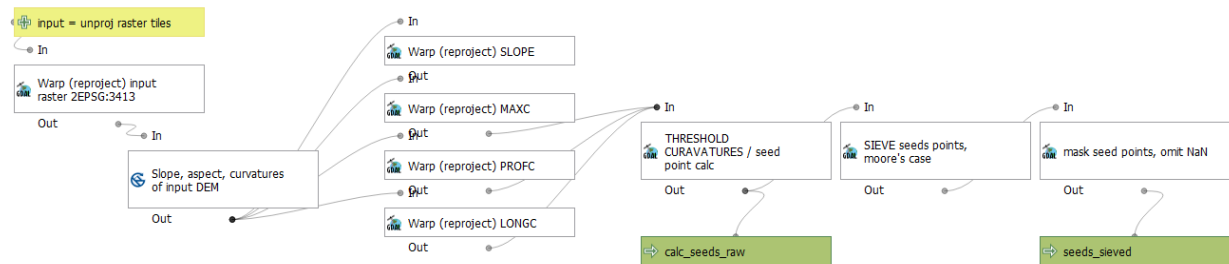


**Figure 3.6** – Graphical model for deriving seed points, which later serve as an input for seeded region growing. The model takes elevation data as input, calculates slope and surface curvatures, and reprojects the layers to the project CRS. Finally, the cells meeting a certain criterion are extracted and sieved.

aspect and different curvatures for each raster cell. The configuration options include seven different calculation methods for slope, aspect and curvature. Three of these seven methods are utilized and their results are compared to determine which methods performs best for the purpose. Unfortunately, the output files of all SAGA modules are left without CRS. Thus, after using a SAGA algorithm I reproject each raster tile according to the instructions in section 3.2.3 before advancing. I then instruct `gdal_calc.py` to assign the value 1 to every raster cell that meets the requirements in eq. (3.1). All other cells are assigned *nodata*, which results in a seed point mask representing esker ridge lines. However, the image is still noisy due small clusters of outliers that do not belong to a ridge but other topographic eminences . This cluster can be filtered out using `gdal_sieve.py`.

### Parameterisation into different terrain parameters

In summary, the landform type that I am interested in is a ridge with characteristic heights, widths, lengths, sinuosity and slope gradients. These information correspond to different terrain parameters which can be allocated to groups of 0, 1st and 2nd order differentials. Ridges serve as seed points for the planned region region algorithm and are thus the first concern in the process of esker extraction. Ridge detection is connected to a combination of different surface curvatures, more specifically we can expect a raster cell to be part of a ridge line if both its profile curvature and longitudinal curvature are convex. In a logical context, this would translate to

$$\text{if } (PROFC \times LONGC) > 0 \rightarrow P(x,y) \in RidgeLine \quad (3.1)$$

where PROFC is profile curvature, LONGC is longitudinal curvature,  $P(x,y)$  is a raster cell at location  $(x,y)$  and *RidgeLine* is a set of raster cells representing ridge lines within the raster extent.

### 3.2.6 Seeded Region Growing

Having found seeds for the region growing procedure, I can now funnel them into SAGA's Seeded Region Growing module (Adams and Bischof (1994) and Bechtel, Ringeler, and Böhner (2008)). This

tool takes as input the *seeds* in grid form generated as described in the section before, and **features** as a grid list. For this grid list one can select the raster layers the growing of the regions should be based upon. This way I can incorporate the terrain parameters than cover esker height, slope gradient and esker width by adding the layers that contain elevation and slope values as input **feature**. Simultaneously, I need to adjust the numbers for **variance in position space** and **variance in feature space**. The latter corresponds, in this example, to the deviation in elevation or slope gradient between the initial seed points and the most outer cells added to the region. In this way maximum esker height and maximum slope gradient are accounted for. **Variance in position space** on the other hand manages maximum esker width, as it represents the difference in horizontal distance similar to a buffer. However, the unit is in grid cells. When working with 2 metre grid resolution, a value of 37.5 translates to 75 metres horizontal growth around the initial seed point. As esker display a width smaller than 150 metres in 99% of all cases (Storror, Jones, et al. 2021), I chose a maximum horizontal growth of 75 metres. Furthermore, the algorithm was ordered to search in all eight neighbouring cells (Moore's case) for new cells to add to the growing region. Other important input variables are the similarity threshold. The similarity threshold limits the region growing process in terms of how similar a cell has to be in order to be part of the growing region. T

The output of the seeded region growing algorithm includes three files: similarity, segments and seeds. the similarity file is of main interest, as it contains the cell compounds representing eskers. The cell values theoretically range from  $[0, 1]$ , with 1 reflecting a maximum similarity with the initial seed points and 0 no similarity whatsoever. The actual cell values only show a range of  $[0.5, 1]$  as I defined `similarity threshold = 0.5`.

### 3.2.7 Postprocessing

In order to account for eskers being elongated features, I want to filter out and remove regions in the outcome that are round, rather than being elongated. Wu, Merchant, and Castleman (2008) propose a calculation for *thinness*, which is a method from image processing, but related to the filtering of sliver polygons in GIS. The underlying is to relate a polygon's area with its perimeter. Using eq. (3.2) a perfect circle is assigned a value of 1, other shapes result in values between 0 and 1.

$$Thinness = 4 \cdot \pi \cdot \frac{area}{perimeter^2} \quad (3.2)$$

Before thinning, the raster regions are vectorized, the boundaries of adjacent polygons are dissolved and possible "holes" are filled, Then, their geometries are being checked and fixed if needed. If the regions' and thus the resulting polygons' boundaries are severely rutted, I will apply a 10 metre buffer around them. This temporary buffer is only used for the calculation of thinness and to remove region that are not thin enough, and deleted later.

### 3.2.8 Validation

The previous step leaves us with cell compounds modelling the shape and extent of eskers. To assess the quality of my work I will compare these cell compounds to the reference map of ridge lines of Canadian eskers from Storrar, Stokes, and D. J. Evans (2013). There are several options conceivable for this comparison. A simple, yet effective approach is to match the length of all reference esker ridge lines against the ridge line segments that lie within the grown regions. This allows a statement regarding the amount of esker ridge lines in the reference data set that were correctly detected. For this end, I first need to convert the grown regions, which are still in raster data format, into polygons. Then I check for invalid geometries in these polygons and fix them, if needed. At the same time I extract those reference esker ridge lines by the extent of the raster layer currently working on. Their total length over that areal unit is being calculated and stored as an attribute (`l_all_m`). Again, I check for empty geometries and remove them. It is now that an intersection between reference esker ridge lines and polygons from region growing is possible. The outcome are line segments that lie within the grown region, I can measure their total length and save them as an additional attribute (`l_intersec_m`). The ratio of both these new attributes represents the fraction of correctly detected esker ridge lines (eq. (3.3)).

$$\frac{\text{length\_intersec\_m}}{\text{totlength\_m}} = \text{ratio\_length} \in [0, 1] \quad (3.3)$$

$$\frac{\text{area\_intersec\_m}^2}{\text{totarea\_m}^2} = \text{ratio\_area} \in [0, 1] \quad (3.4)$$

## Results

This chapter describes the results obtained by applying the methods described in chapter 3.

First, I removed DEM cells with a TRI above the threshold value according to section 3.2.3. Then, the pre-existing nodata areas and the newly assigned nodata areas post-TRI were both filled with GRASS's `r.fillnulls`. Depending on the number and size of the holes in each virtual raster tile, this could be the most time consuming step in the whole workflow. Figure 4.1 shows an exemplary region with an area holding nodata values (*Notable Area 1*) and an eskers segment missing in the data recorded by Storrar, Stokes, and D. J. Evans (2013) (*Notable Area 2*).

### 4.1 Combination of Morphometric Parameters and Sieving Threshold: Influence on Accuracy

Second, raster layers representing geomorphometric parameters such as slope or different curvatures were calculated using SAGA's `Slope`, `Aspect`, `Curvature`. The algorithm offers seven calculation methods for curvature values, of which I tested three more thoroughly. Table 4.1 displays the comparison between three calculation methods offered by the algorithm: I. S. Evans (1979), Zevenbergen and Thorne (1987), and Florinsky (2009). The thresholds for seed point sieving are denoted by the numbers in subscript. I.e. a threshold of 50 means only seed clusters with a count of 50 adjacent cells or higher are kept for region growing. Checking for adjacency of a cell to a cluster was performed in a Moore's case scenario.  $L_{\text{int}}$  is the summed lengths of intersection between eskers mapped by Storrar, Stokes, and D. J. Evans (2013) and my polygons from seeded region growing.  $L_{\text{ratio}}$  represents the ratio between  $L_{\text{Intersection}}$  and total length of all eskers mapped by Storrar, Stokes, and D. J. Evans (2013) within the given raster tile. Furthermore, the area of polygons from seeded region growing that do not touch an esker ridge line mapped by Storrar, Stokes, and D. J. Evans (2013) is summed up ( $A_{\text{int}}$ ) and compared to the total area of seeded regions within the given raster tile ( $A_{\text{ratio}}$ ). In other words  $L_{\text{int}}$  represents the length of eskers ridge lines in the reference data set that were detect

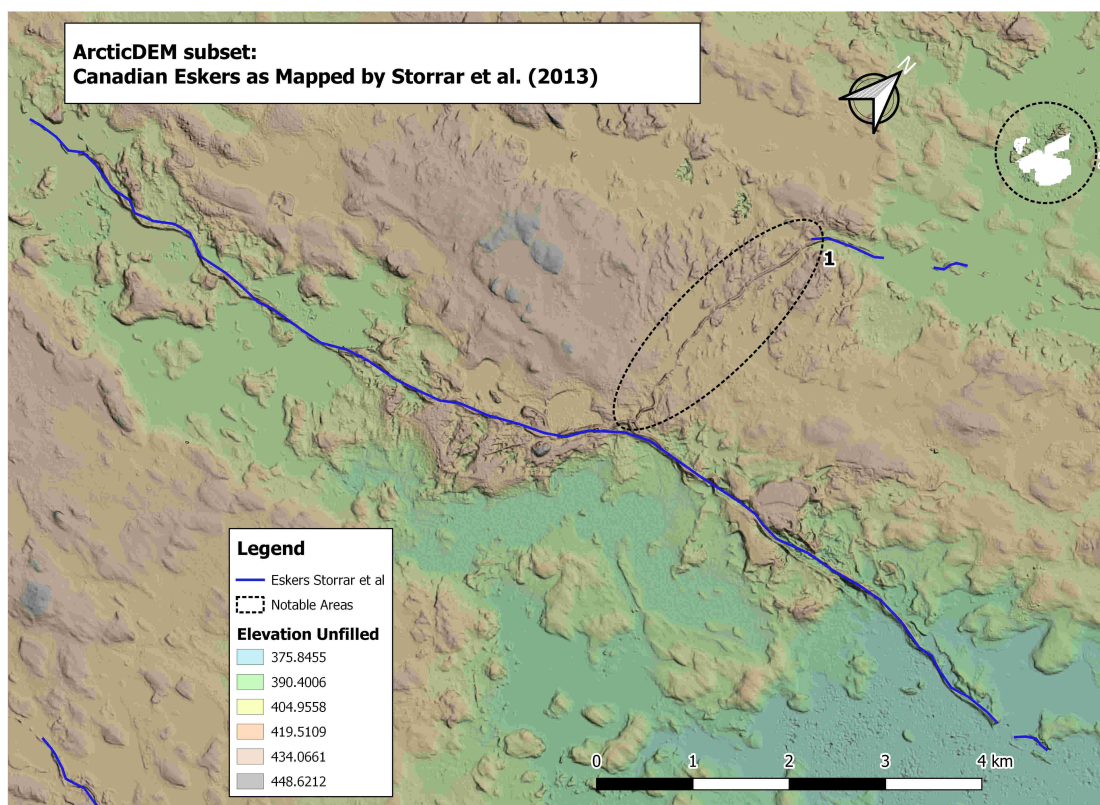


**Figure 4.1** – ArcticDEM subset of sub-tile 26\_12\_2\_1 and esker ridge lines mapped by Storrar, Stokes, and D. J. Evans (2013). Notable area 1 depicts a region where a ridge was not identified as an esker by the reference data set by Storrar, Stokes, and D. J. Evans (2013), notable area 2 displays an area with nodata values for elevation.

by my method and indicates the accuracy of the presented approach. On the other hand,  $A_{\text{int}}$  reflects the area mapped by my method which is also considered part of an esker by the reference data set and therefore gives an estimate on how much area was correctly sampled as belonging to an esker. I did find the method by I. S. Evans (1972) with a sieve-threshold of 75 to be optimal based on the numbers presented in table 4.1 and a qualitative assessment of the resulting seeded regions (compare section 4.2 and section 4.2 for reference).

## 4.2 Seed Generation & Ridge Detection

After settling for a calculation method for geomorphometric parameters, I combined profile curvature, longitudinal curvature and maximum curvature to obtain seed points representing esker ridge lines. This combination of curvatures to yield a specific landform is described in section 3.2.4. Section 4.2 shows the raw seed points and section 4.2 shows the seed points after sieving for the example subset. Note how well the seeds follow a ridge line that was not mapped by Storrar, Stokes, and D. J. Evans (2013) as an esker (*Notable Area 1* in fig. 4.1), but struggles to detect the entire length of the longer

**Table 4.1** – Outcome of seeded region growing based on three different calculation methods within SAGA’s **Slope**, **Aspect**, **Curvature** algorithm. Numbers in subscript depict the threshold value used for seed point sieving. The total length of all eskers mapped by Storrar, Stokes, and D. J. Evans (2013) amounts to 15.61 kilometres, the total area of the subset used for the analysis in this table is equal to 101.06 square kilometres.

Method	$L_{\text{int}}$ [km]	$L_{\text{ratio}}$ [%]	$A_{\text{tot}}$ [km <sup>2</sup> ]	$A_{\text{int}}$ [km <sup>2</sup> ]	$A_{\text{ratio}}$ [%]
Evans <sub>50</sub>	9.44	60.47	2.30	2.03	88.38
Evans <sub>75</sub>	8.20	52.49	1.85	1.68	91.13
Evans <sub>100</sub>	6.27	40.18	1.43	1.35	94.27
Evans <sub>150</sub>	4.98	31.92	1.07	1.04	96.87
Zevenbergen <sub>50</sub>	9.81	62.85	2.46	2.12	86.17
Zevenbergen <sub>75</sub>	8.18	52.37	1.89	1.70	90.08
Zevenbergen <sub>100</sub>	6.77	43.36	1.55	1.44	92.91
Zevenbergen <sub>150</sub>	4.97	31.85	1.10	1.07	97.05
Florinski <sub>50</sub>	6.44	41.25	1.47	1.29	87.88
Florinski <sub>75</sub>	5.73	36.70	1.15	0.95	83.08
Florinski <sub>100</sub>	4.30	27.55	0.83	0.71	85.79
Florinski <sub>150</sub>	2.80	17.94	0.48	0.43	89.09

ridge stretching from north-east to south-west.

### 4.3 Seed Region Growing & Postprocessing

Due to the way SAGA’s **Seeded Region Growing** accepts input parameters, simultaneous implementation of all desired morphometric parameters was not possible. For this reason, two SRGs were performed parallel, their resulting layers were stacked and the values were normalized to fit within the probability range of  $P = [0, 1]$ . Figure 4.3a shows the SRG result based on slope, elevation and horizontal distance. Figure 4.3b shows the SRG result based on profile curvature and horizontal distance. Figure 4.4 shows the fusion of all considered parameters. Please note how rutted the boundaries of the stacked SRG are compared to the SRG based on only slope and elevation.

As a means of post-processing, the form of the resulting seeded regions was checked. In a first step, the raster cell compounds were vectorized, adjacent polygons were merged and resulting holes and sliver polygons were removed and filled. As esker ridge lines are elongated, polygons with a round shape are thought to result from peaks rather than ridge lines. Which is why polygons with a thinness (section 3.2.7) higher than 0.75 were removed. As described before, the polygons were given a 10 metre buffer to cancel out the effect of the rutted boundaries on a region’s perimeter. Then,

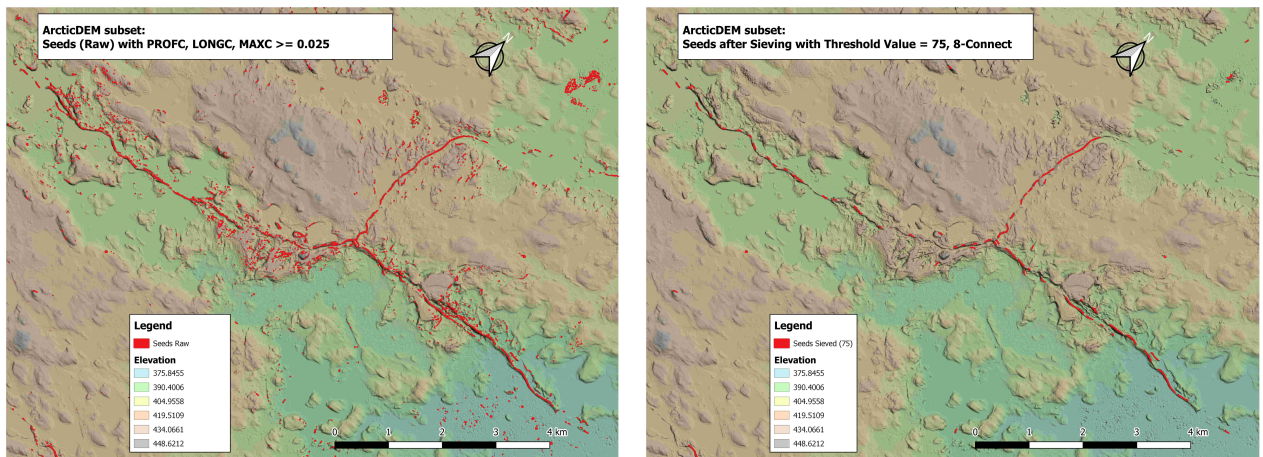


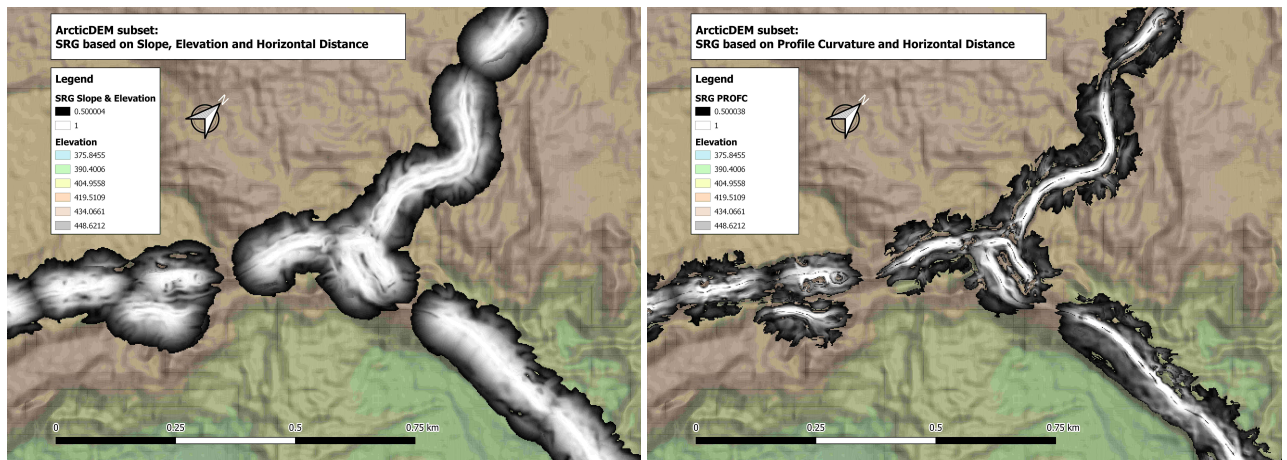
**Figure 4.2** – Raw seed points and seed points after sieving for exemplary region.

all elongated polygons are matched with the original raster cell compounds from SRG: Figure 4.4b displays the SRGs that are kept for further analysis alongside with the polygons I used to remove roundish regions (red).

## 4.4 Validation of Results

Finally, I compared the detected eskers with esker ridge lines mapped by Storrar, Stokes, and D. J. Evans (2013), and assessed characteristics of the extracted eskers and esker segments. One qualitative and vivid way of seeing if the found regions drape eskers is to generate a 3D-view. Two examples of this are shown below. fig. 4.5 exhibits an example where my prediction fits the terrain and the reference ridge line well. Notice how the reference ridge line (blue) diverges from the actual ridge line observable from the coloured DEM. However, fig. 4.6 shows an example of an artefact, where a convex landform was incorrectly .





(a) SRG based on difference in slope, elevation and horizontal distance. Variance in feature space = 25, variance in position space = 37.5, similarity threshold = 0.5  
 (b) SRG based on difference in profile curvature and horizontal distance. Variance in feature space = 0.045, variance in position space = 37.5, similarity threshold = 0.5

Figure 4.3 – SRG based on different input parameters for exemplary region.

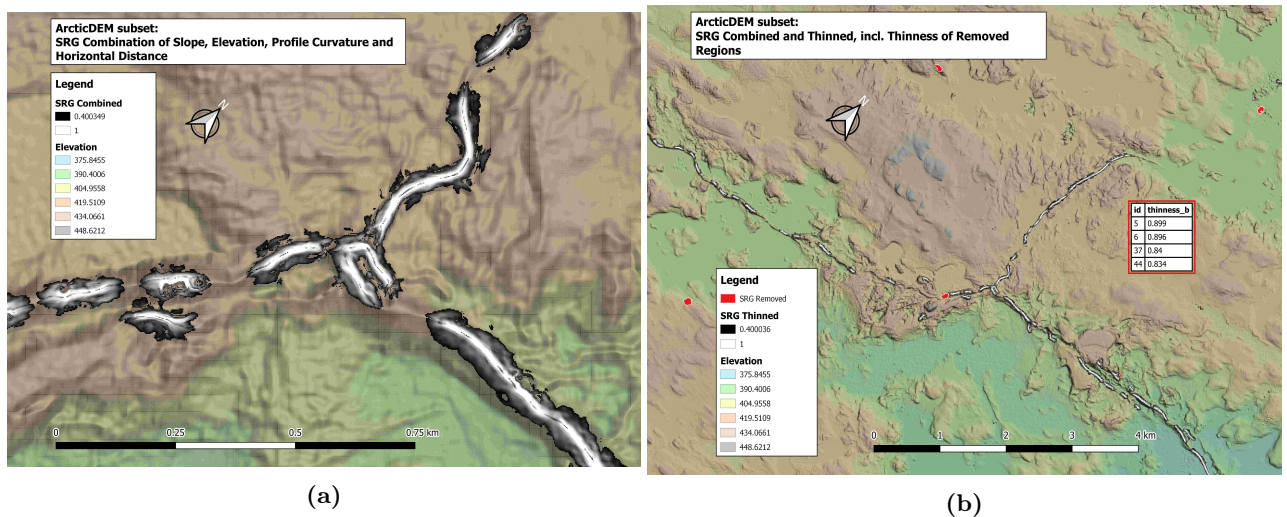
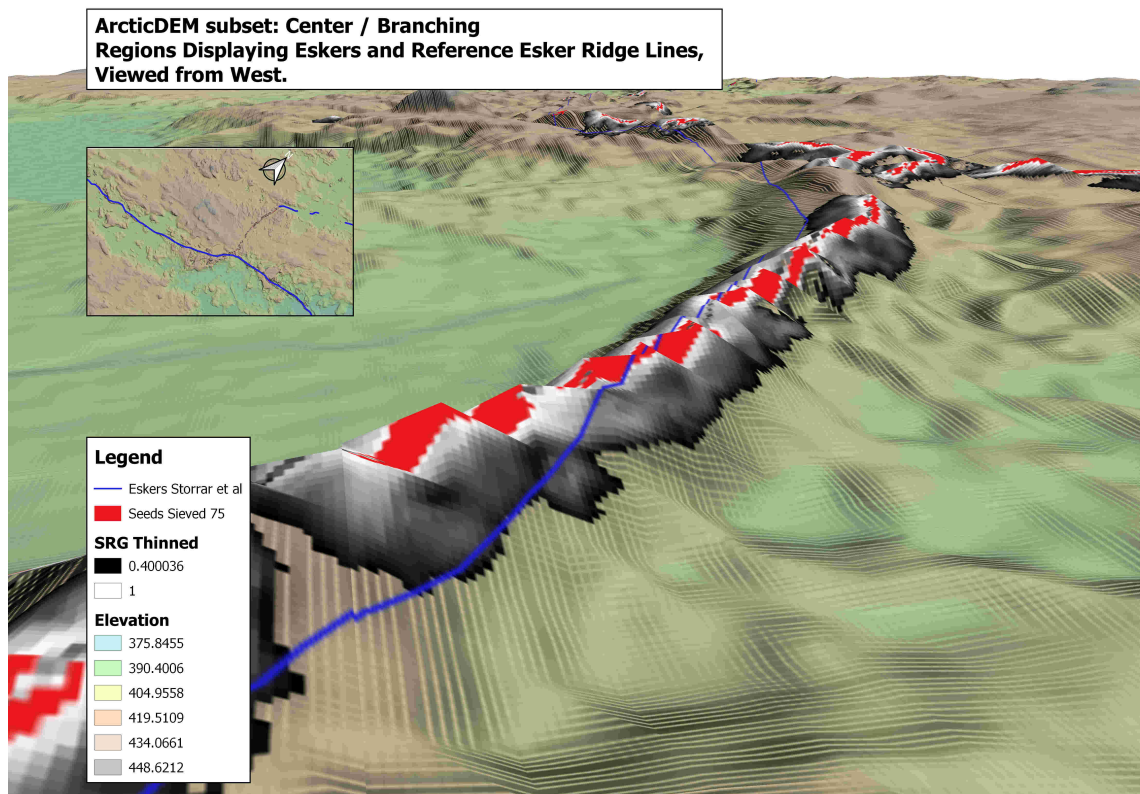
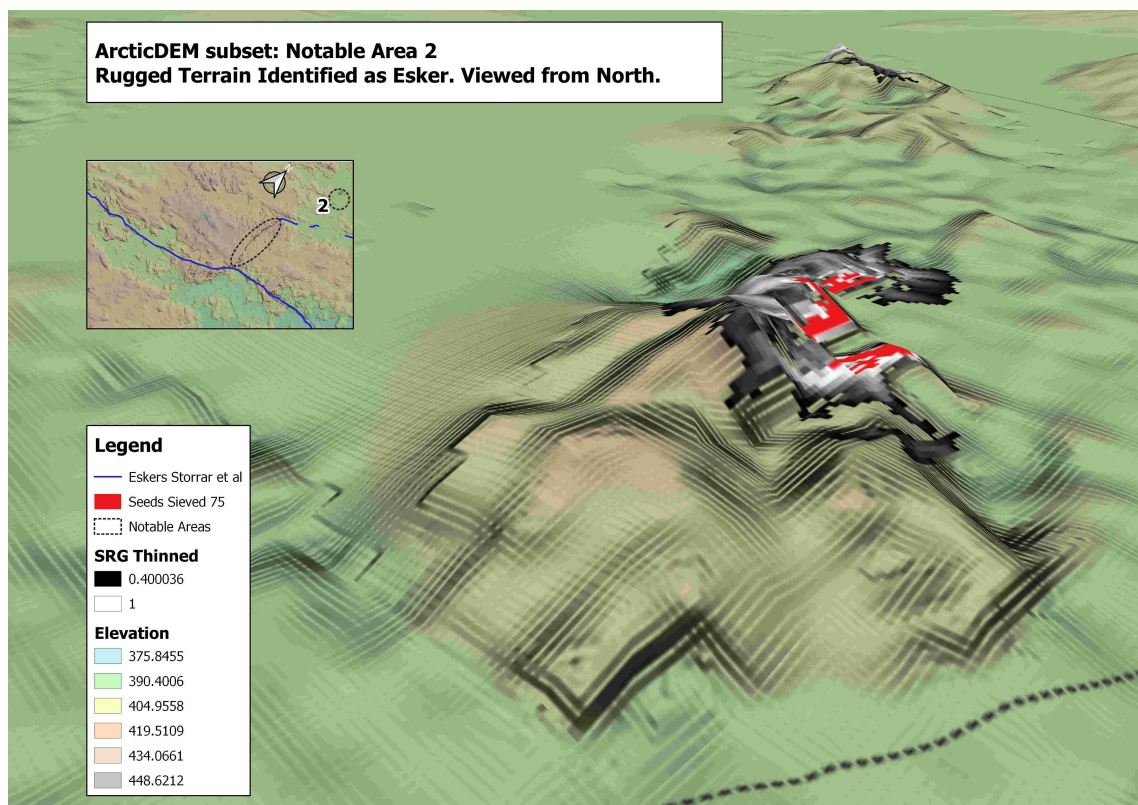


Figure 4.4 – SRG with combined parameters (slope, vertical and horizontal distance, profile curvature), versus combined and thinned SRG for exemplary region.



**Figure 4.5** – 3D-view of regions from SRG, with superimposed seed points and esker ridge lines from Storrar, Stokes, and D. J. Evans (2013). Vertical scale inflated by factor 2.



**Figure 4.6** – 3D-view of a convex landform incorrectly detected as an esker at the edge of a former nodata field in *Notable Area 2* from fig. 4.1. Vertical scale inflated by factor 2.

## Discussion

This chapter discusses the results presented in the previous chapter and puts it into context with existing literature. Then, I list constraints regarding the chosen methodology and regarding the data sets used for this work. The last section gives an outlook on future research and, by doing so, bridges the gap between previous written work, my contribution and future research.

### 5.1 Interpretation of Results

#### 5.1.1 Combination of Morphometric Parameters and Sieving Threshold: Influence on Accuracy

There are several factors that determine how closely the calculated seed points mimic the ridges lines. On the one hand, the method of calculating slope and curvature is crucial (Wood 1996; Straumann 2010). Also, the size of the search window plays a decisive role as well as the spatial resolution of the data set the algorithm is performed on. SAGA's *Slope*, *Aspect*, *Curvature* provides algorithms from seven different scholars using second or third order derivatives, and all of them yield differing results. Varying of the size of the search window manually is not possible with this process. The challenge is the combination of resulting curvatures to receive cells with desired topographic characteristics. Wood (1996) proposed three different feature classification criteria for ridges:

- i)  $Slope = 0 \cap MAXC > 0 \cap MINC = 0$
- ii)  $Slope > 0 \cap CROSC > 0 \cap LONGC = 0$
- iii)  $Slope > 0 \cap CROSC = 0 \cap LONGC > 0$

The first criteria listed above is backed up by Straumann (2010) who also uses a combination of

- iv)  $MAXC > 0 \cap MINC = 0$

to describe ridges. However, none of the above i) - iv) yielded usable results, so I started to experiment with the curvature layers, and surveyed breaks in MAXC, LONGC and PROF C using the profile tool

in QGIS. An exemplary transect through an esker is shown in fig. 5.1. I found that seed points best matched ridges when using the following expression:

$$PROFC \geq 0.025 \cap MAXC \geq 0.025 \cap LONGC \geq 0.025 \quad (5.1)$$

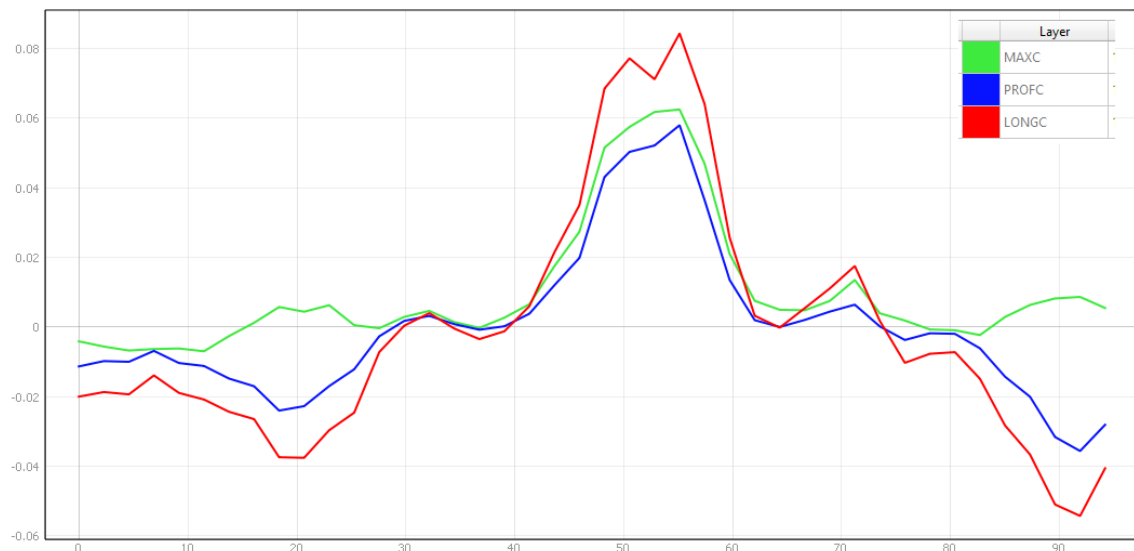


**Figure 5.1** – Transect through exemplary esker, using the profile tool plug-in in QGIS. The x-axis represent metres in horizontal distance, while the y-axis represent values for different morphometric parameters based on 2<sup>nd</sup>-order derivatives.

The result of this raster calculation is illustrated in section 4.2. My work shows that this approach and these specific thresholds allow to sample and classify a big part of actual ridge lines. However, it also classifies many pixels that cannot be considered part of ridge lines. As these miss-classified pixels usually build smaller, non-contiguous clusters, I introduced a rule for sieving out cluster sizes above a specific threshold. In fig. 5.2 I present the numbers from table 4.1 in a graphic to illustrate the relationship between the sieving threshold and the accuracy regarding intersection with the esker ridge lines mapped by Storrar, Stokes, and D. J. Evans (2013). The curvature calculation methods by I. S. Evans (1979) and Zevenbergen and Thorne (1987) perform about equally well and we can see an almost linear relationship between the two methods when varying the value for seed point sieving. As I aimed for at least 50% intersection in length for the test subset, the decision was made in favor of Evan’s method with a sieving threshold of 75 cells. Unfortunately, the method by Florinsky (2009) yielded worse results. The ascent with a sieve threshold of 50 cells with Florinski’s method can be explained as follows: Due to a lowered threshold for sieving, more regions are generated. More spawned regions leads to a higher probability of regions merging together. A region in fig. 4.1, Notable Area 2, newly merged with a region that is intersected by a ridge line from the reference data set. Which leads to a disproportional area added to  $A_{int}$ .

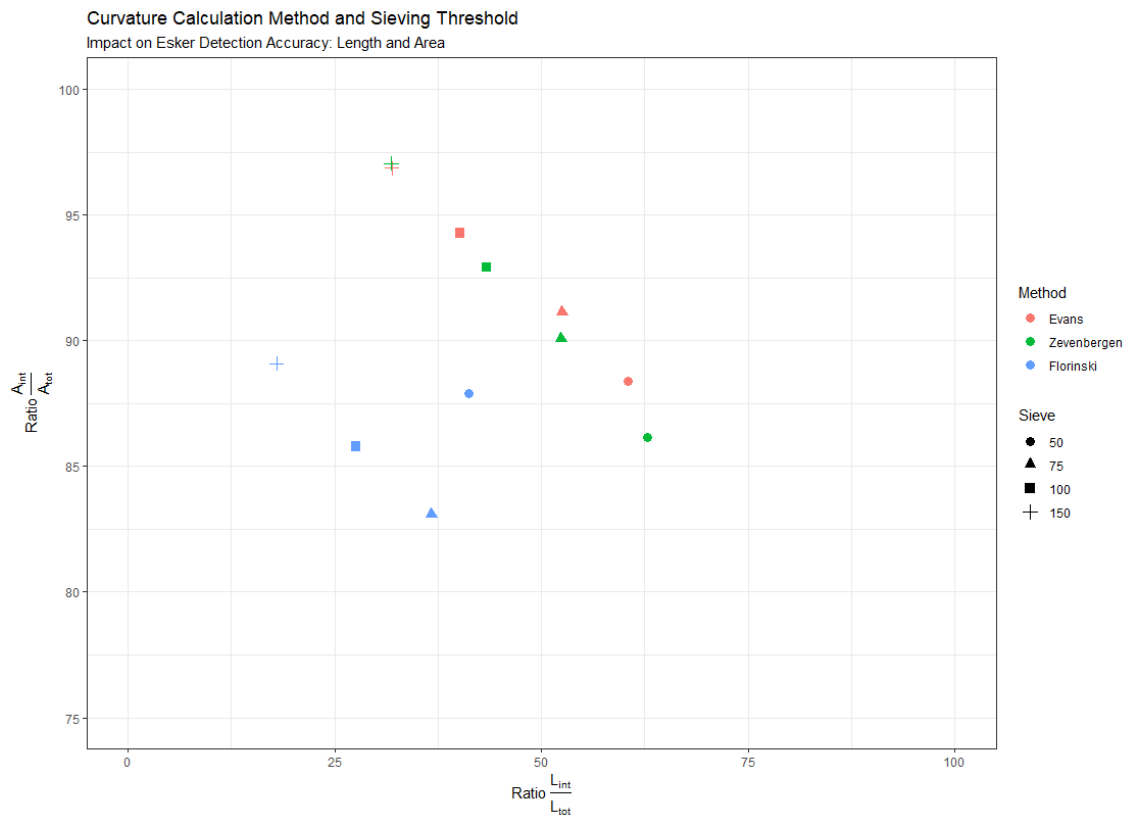


**Figure 5.2** – The figure is an illustration of table 4.1, displaying the three tested calculation methods by I. S. Evans (1979), Zevenbergen and Thorne (1987), and Florinsky (2009). The y-axis displays the ratio between mapped regions that are intersected by esker ridge lines of the reference data set by Storrar, Stokes, and D. J. Evans (2013) and the total area of mapped regions within the subset presented in fig. 4.1. The x-axis displays the ratio of esker ridge length mapped in the reference data set by Storrar, Stokes, and D. J. Evans (2013) that was intersected by my mapped regions versus the total length of esker ridge lines from the reference data set. The values apply to the extent displayed in fig. 4.1.

## 5.2 Methodological Limitations

Due to the combination of methods chosen for esker extraction from a DEM, certain limitations inherit to this approach need to be addressed. These are, on the one hand, the fact that the search for this specific landform is based on shape and therefore only on geometric properties. Furthermore, I found certain limitations due to the choice made regarding software. These aspects are explained below.

### 5.2.1 Focus on Geomorphometric Characteristics

With the focus on geometrical characteristics of the landform I ignored other properties inhere to eskers. For example, there area certain prerequisites regarding subsoil where eskers can emerge. Even though they can form on top of sediments, they are more likely to occur in regions with harder

substrates. It would have been possible to incorporate geological maps of Canada (e.g. Fulton (1995), Gowan et al. (2019)). The latter of the two sources provides a shapefile containing data on underlying rock types in North America. Predicting occurrence of eskers based on geology was not part of this thesis, but should be considered in a further step.

Moreover, the methodology presented in this thesis does not respect the fact that eskers are sinuous and elongated landforms. Adding the idea of thinness (Wu, Merchant, and Castleman 2008) as measure for a polygon's ratio between area and perimeter is an attempt to address the elongation of eskers. But it rather helps to remove roundish polygons than finding actual elongated ones. My approach lacks the idea and recognition of an alignment of the SRGs, based on which regions belonging to the same esker could be linked and would thus become thinner.

### 5.2.2 Software Constraints

Opting for QGIS and especially QGIS' graphical modeler as the main processing tool presented advantages as well as drawbacks. Due to being an open-source software, it would run locally on my personal computer. It offers great functionality with its pre-installed providers and an extensive plug-ins library. The graphical modeler is a comprehensible, yet powerful application with a GUI, which is accommodating for testing short chains of processing algorithms while providing an overview of the workflow. However, when working with larger chains of processing algorithms, the graphical modeler loses many of its advantages. The virtue of overview given by the flowchart-like appearance is crippled. Version control is somewhat confusing, as it is not always obvious where the model currently performing changes or is being saved. Also, only partially running a model or copying and pasting a part of an existing model into a new model is not an option, as dependencies between the processing steps are messed up. Furthermore, running a self-made model as batch-process is possible, but changing input parameters and handling output file names is not as efficient as in a coding environment.

Moving on, I would like to address the documentation of QGIS in general, but SAGA as an algorithm provider in particular. QGIS, GRASS and GDAL provide decent documentation for their algorithms, be it within the QGIS GUI or the written manual. Oftentimes, theoretical explanations of a processing step could be found in more detail at ESRI's website. SAGA, however, as powerful and extensive as it is, oftentimes gives very little guidance on what a specific algorithm does. Input parameters are not well explained and the manual refers - if at all - to papers in which the algorithm was originally implemented.

## 5.3 Data Limitations

### 5.3.1 ArcticDEM

It should be well established by now that ArcticDEM only covers landmass above 60° North, which is an obvious limitation to mapping eskers located further south. Moreover, there are artefacts within the data that evidently propagate into the analysis of elevation-derived measures. Despite the sampling of the best-quality DEM strips for DEM mosaics (Porter et al. 2018), there is an extensive amount of nodata areas, and few areas that show a jump of about 100 metres vertical distance within a difference of 10 metres in horizontal direction (see fig. 5.3). Most nodata areas are affiliated with water bodies, which is fine for interpolation of the elevation values and in line with Storrar, Stokes, and D. J. Evans (2013), where it is stated that esker tails are often connected to lakes or kettle holes. At the edge of nodata areas, however, short sub-linear hills presented themselves which did not match the reference data set on Canadian eskers or the qualitative assessment of the regions found through this work.

Overall, the following weaknesses that were also described by Porter et al. (2018) became apparent throughout the project:

- It is no “bare earth” product. The underlying imagery utilized for DEM generation does include vegetation or man-made surface features. This aspect was ignored under the assumption that man-made settlement are either absent in the study area or easily detectable.
- The underlying imagery is optically derived, so atmospheric obstructions in the form of clouds and shadows are possible, which obscure terrain.
- The product is not “eyes on” or was not manually edited. False landforms and DEM anomalies may exist and persist in my data, despite the attempt to mitigate anomalies by filtering out cells with a large terrain ruggedness index value.
- Data management was problematic when handling tiles with a resolution of 2 metres. I pointed out the difference in size in table 3.1 and explained how I re-sampled the default sub-tile into 25 VRTs due to the fact that my personal computer’s RAM was overwhelmed by the size of a raster file with an edge length of 25 kilometres.

### 5.3.2 Reference Data Set on Eskers

As pointed out in section 3.1.2, the mapping of the reference data set on Canadian eskers was performed manually by varying spectral band combinations and scales. The ETM+ data has a resolution of 30 metres (or 15 metres in the panchromatic band, respectively). Given that the source data is more coarse than the elevation data I used, the segments of their resulting esker ridge lines does not closely follow the actual ridge lines based on the ArcticDEM. The map by Storrar, Stokes,



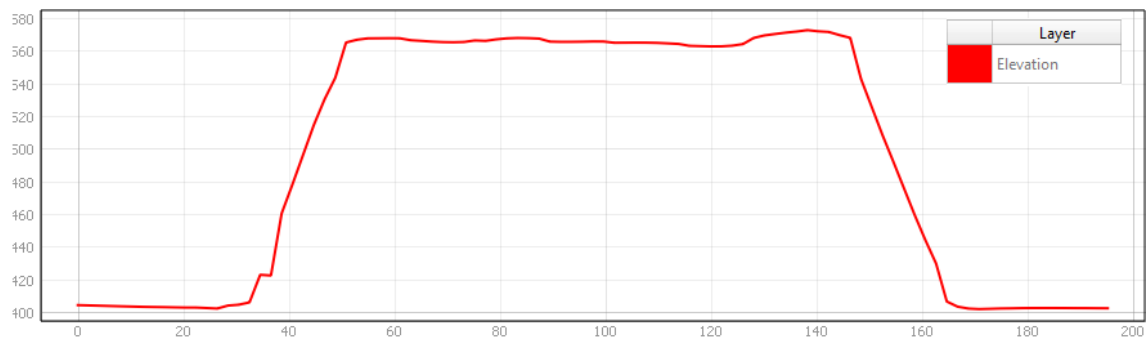


**Figure 5.3** – Transect through subjective artifact in elevation data in southern part of ArcticDEM sub-tile 26\_12\_2\_1, using the profile tool plug-in in QGIS. Axis values in metres.

and D. J. Evans (2013) generally links segments of esker ridge lines that belong together better than my approach. This is a methodological constraint which was pointed out above. However, there are ridge lines apparent in the ArcticDEM that are not mapped as eskers in their map that could be identified with the presented approach. One example of a missing esker ridge line with a length of 3 kilometres is given in fig. 4.1. Therefore, using the "Map of large Canadian Eskers" as reference data set was found to be valuable for the accuracy of my work. Meaning that a discussion regarding the resulting intersection ratios (e.g. table 4.1, fig. 4.1) should be more considered with the precision of the reference data set.

## 5.4 Outlook

In this section I would like to give possible trajectories for future research and discuss ways in which the existing approach for esker extraction can be improved.

### Methodological Outlook

First, I think the procedure presented in this thesis can be improved at three specific instances. These steps include the process of finding seed points, the parameters used for region growing and linking of detached regions that belong to the same landform entity, i.e. the same esker.

Finding more fitting seed points for region growing would enhance the overall accuracy, as this step is the most crucial input for the entire procedure. If a ridge segment is not provided with a seed point, there will be no region growing at that point and therefore the esker segment is not being mapped or extracted. More predictive seed point could be achieved by an extensive study of surface curvatures, and consequently more effective selection criteria for curvatures and curvature thresholds. Furthermore, there are more information available on esker characteristics (Storror, Jones, et al. 2021) than the one included in my model. The topic of sinuosity was left untouched, as well as typical ratios between segment length and sinuosity or the ratio between height and width. However, applying

further criteria or thresholds connected to esker segment length is only fruitful after incorporating the third and most delicate suggestion for improvement: The bridging of gaps between esker as described by Lewington, Livingstone, Sole, et al. (2019) to improve the longitudinal completeness. With this, the absence of seed points along an esker ridge and resulting gaps between esker segments can potentially be *bridged* or closed.

### **Thematic Outlook**

With more precise mapping of specific glaciological landforms, process models for esker formation, sediment flux in subglacial channels and glaciers dynamics in general can be improved (Storrar, Stokes, and D. J. Evans 2014b; Storrar, Jones, et al. 2021). Also, eskers usually do not emerge as isolated landforms, but are embedded in elongated tracts of hummocks or so called hummock corridors (Lewington, Livingstone, Sole, et al. 2019). Better models regarding the spatial distribution and volume of eskers, or e.g. inclination of their ridge lines allow to model surrounding and hydraulically connected landforms and processes in more detail. As the domain of the ArcticDEM extends beyond the Canadian border, mapping of other regions within the Arctic is possible with the same data set and the approach present in this thesis. For example, Lewington, Livingstone, Sole, et al. (2019) and PGC (2021) have studied eskers in Finland as well, providing ways of extraction of their spatial properties using elevation data from ArcticDEM.

## Conclusion

The ArcticDEM was used as a main data source for this project. It provides interesting opportunities for research in glaciology and geomorphology. In this thesis, I exhibit a method to delineate esker segments in the northern part of Canada by applying techniques from geomorphometry and a region growing procedure. The method succeeded in detecting esker ridge lines that have not been mapped in the reference data set fig. 4.4b. However, it performs less well in detecting the entire length of longer ridge lines. This is shown in an extensive comparison of different calculation methods within the used SAGA algorithm. The external validity of my model is not tested, as it has only been applied to an area of 2500 square kilometres in the McCann Lake region, south-east of the former Keewatin Ice Divide. However, the results show that the ArcticDEM can be used to identify landforms such as eskers. Therefore, the presented method and results can contribute to existing findings in related fields of research by answering the research questions stated in chapter 1. Future work should further reflect on the process of finding seed points, the parameters used for region growing and more elaborate options of linking detached regions that belong to the same landform entity.

Besides the results, there are two main personal lessons learned. One, the crux of working with automatically generated elevation data with no manual postprocessing on behalf of the provider. Related to that is the importance of preprocessing elevation data to fit the users demands. And second, the size of data and thus calculation time vary drastically with different resolutions. As obvious as it may seem, balancing the extent of a raster between sufficient sample size and efficient calculation times for testing is a challenging. Finally, this project has been motivated by the release of the ArcticDEM and demonstrates an interesting option of its application in field of glaciology and geomorphometry.

# Appendices

# Appendix A

## Dictionaries, Data & Software

**Table A.1** – Overview of data sets used in the context of this thesis and their respective source.s

Data Set	Source	last accessed
ArcticDEM	<a href="https://data.pgc.umn.edu/elev/dem/setsm/ArcticDEM/">https://data.pgc.umn.edu/elev/dem/setsm/ArcticDEM/</a>	24.02.2022
eskersCA.shp	<a href="https://www.researchgate.net/publication/284715993_Canadian_eskers_shapefile">https://www.researchgate.net/publication/284715993_Canadian_eskers_shapefile</a>	24.02.2022

**Table A.2** – Overview of software packages and libraries used in the context of this thesis.

Name	Source	Version
GDAL	<a href="https://gdal.org/download.html">https://gdal.org/download.html</a>	3.3.1
GNU wget	<a href="https://eternallybored.org/misc/wget/">https://eternallybored.org/misc/wget/</a>	1.21.2
Map Swipe Tool	<a href="https://www.qgis.org/de/site/forusers/download.html">https://www.qgis.org/de/site/forusers/download.html</a>	3.16.11
Processing Saga NextGen Provider	<a href="https://www.qgis.org/de/site/forusers/download.html">https://www.qgis.org/de/site/forusers/download.html</a>	0.0.7
Profile Tool	<a href="https://www.qgis.org/de/site/forusers/download.html">https://www.qgis.org/de/site/forusers/download.html</a>	4.2.2
Quantum GIS	<a href="https://www.qgis.org/de/site/forusers/download.html">https://www.qgis.org/de/site/forusers/download.html</a>	3.16.11

**Table A.3** – Overview of dictionaries used in the context of this thesis.

Name	Reference	Abbreviation
United States Department of Agriculture: Natural Resource Conservation Service	<a href="https://www.nrcs.usda.gov/wps/PA_NRCSCConsumption/download?cid=nrcs142p2_053182&amp;ext=pdf">https://www.nrcs.usda.gov/wps/PA_NRCSCConsumption/download?cid=nrcs142p2_053182&amp;ext=pdf</a>	USDA
WordNet	<a href="http://wordnetweb.princeton.edu/perl/webwn">http://wordnetweb.princeton.edu/perl/webwn</a>	WNET
Oxford Dictionary of Geography	<a href="https://www-oxfordreference-com.ezproxy.uzh.ch/view/10.1093/acref/9780199680856.001.0001/acref-9780199680856-e-1125?rskey=kX6suX&amp;result=981">https://www-oxfordreference-com.ezproxy.uzh.ch/view/10.1093/acref/9780199680856.001.0001/acref-9780199680856-e-1125?rskey=kX6suX&amp;result=981</a>	ODGeo
Encyclopedia of Planetary Landforms	<a href="https://link.springer.com/referencework/10.1007/978-1-4614-3134-3">https://link.springer.com/referencework/10.1007/978-1-4614-3134-3</a>	EPL
Encyclopedia Britannica	<a href="https://www.britannica.com/">https://www.britannica.com/</a>	EB

# Bibliography

- Adams, Rolf and Leanne Bischof (1994). “Correspondence Seeded Region Growing”. In: *IEEE Transactions on pattern analysis and machine intelligence* 16.6, pp. 641–647.
- Aylsworth, J.M. and W.W. Shilts (1989). “Glacial features around the keewatin ice divide : districts of Mackenzie and keewatin”. In: *Geological survey of Canada Paper 88-24*, 21 p. DOI: [10.4095/126992](https://doi.org/10.4095/126992).
- Bechtel, Benjamin, Andre Ringeler, and Jürgen Böhner (2008). *Segmentation for Object Extraction of Trees using MATLAB and SAGA*. Tech. rep. University of Hamburg, pp. 1–12.
- Britannica Encyclopedia (2008). *Glaciology*. URL: <https://www.britannica.com/science/glaciology>.
- Broscoe, D et al. (2011). “A semi-automated esker detection method ( EDM ) for improved quantification of glaciated landscapes Geological Survey of Canada Technical Note 2”. In: *Geological Survey of Canada Technical Note 2* May 2015, 17 p. DOI: [10.4095/288146](https://doi.org/10.4095/288146).
- Dai, Chunli, Michael Durand, et al. (2018). “Estimating River Surface Elevation From ArcticDEM”. In: *Geophysical Research Letters* 45.7, pp. 3107–3114. ISSN: 19448007. DOI: [10.1002/2018GL077379](https://doi.org/10.1002/2018GL077379).
- Dai, Chunli and Ian M. Howat (2017). “Measuring Lava Flows With ArcticDEM: Application to the 2012–2013 Eruption of Tolbachik, Kamchatka”. In: *Geophysical Research Letters* 44.24, pp. 12–133. ISSN: 19448007. DOI: [10.1002/2017GL075920](https://doi.org/10.1002/2017GL075920).
- Davison, Benjamin Joseph et al. (2019). “The influence of hydrology on the dynamics of land-terminating sectors of the Greenland ice sheet”. In: *Frontiers in Earth Science* 7, p. 10. ISSN: 22966463. DOI: [10.3389/FEART.2019.00010/BIBTEX](https://doi.org/10.3389/FEART.2019.00010/BIBTEX).
- Dehn, Martin, Holger Gärtner, and Richard Dikau (2001). “Principles of semantic modeling of landform structures”. In: *Computers and Geosciences* 27.8, pp. 1005–1010. ISSN: 00983004. DOI: [10.1016/S0098-3004\(00\)00138-2](https://doi.org/10.1016/S0098-3004(00)00138-2).
- Dikau, Richard (1990). “Geomorphic landform modelling based on hierarchy theory”. In: *Proceedings of the 4th international symposium on spatial data handling*. Zürich, Switzerland: Department of Geography, pp. 230–239. URL: [https://scholar.google.com/scholar\\_lookup?title=Geomorphic%20landform%20modelling%20based%20on%20Hierarchy%20Theorie&author=R.%20Dikau&publication\\_year=1990](https://scholar.google.com/scholar_lookup?title=Geomorphic%20landform%20modelling%20based%20on%20Hierarchy%20Theorie&author=R.%20Dikau&publication_year=1990).

- Dyke, A. S. and V. K. Prest (1987). "Late Wisconsinan and Holocene history of the Laurentide Ice Sheet". In: *Geographie Physique et Quaternaire* 41.2, pp. 237–263. ISSN: 07057199. DOI: [10.7202/032681AR](https://doi.org/10.7202/032681AR).
- Erikson, Mats (Aug. 2003). "Segmentation of individual tree crowns in colour aerial photographs using region growing supported by fuzzy rules". In: *Canadian Journal of Forest Research* 33.8, pp. 1557–1563. ISSN: 00455067. DOI: [10.1139/X03-062](https://doi.org/10.1139/X03-062). URL: <https://cdnsciencepub.com/doi/abs/10.1139/x03-062>.
- (2004). "Segmentation and classification of individual tree crowns : in high spatial resolution aerial images". PhD thesis. Uppsala: Sveriges lantbruksuniv. ISBN: 91-576-6704-7.
- Erikson, Mats and Kenneth Olofsson (2005). "Comparison of three individual tree crown detection methods". In: *Machine Vision and Applications* 16.4, pp. 258–265. ISSN: 1432-1769. DOI: [10.1007/S00138-005-0180-Y](https://doi.org/10.1007/S00138-005-0180-Y). URL: <https://link.springer.com/article/10.1007/s00138-005-0180-y>.
- Evans, David J. A. (2018). *Glaciation : a very short introduction*. Oxford University Press. ISBN: 9780198745853.
- Evans, Ian S. (1972). "General geomorphometry, derivatives of altitude, and descriptive statistics". In: *Spatial Analysis in Geomorphology*. Ed. by Richard J. Chorley. 1st ed. London: Harper & Row, pp. 17–90. ISBN: 9781000000252. DOI: [10.4324/9780429273346-2/GENERAL-GEOMORPHOMETRY-DERIVATIVES-ALTITUDE-DESCRIPTIVE-STATISTICS-IAN-EVANS](https://doi.org/10.4324/9780429273346-2/GENERAL-GEOMORPHOMETRY-DERIVATIVES-ALTITUDE-DESCRIPTIVE-STATISTICS-IAN-EVANS). URL: <https://www.taylorfrancis.com/chapters/edit/10.4324/9780429273346-2/general-geomorphometry-derivatives-altitude-descriptive-statistics-ian-evans>.
- (1979). "An integrated system of terrain analysis and slope mapping (1979 edition)". In: University of Durham, pp. 17–90. URL: [https://openlibrary.org/books/OL19503146M/An\\_integrated\\_system\\_of\\_terrain\\_analysis\\_and\\_slope\\_mapping](https://openlibrary.org/books/OL19503146M/An_integrated_system_of_terrain_analysis_and_slope_mapping).
- (2012). "Geomorphometry and landform mapping: What is a landform?" In: *Geomorphology* 137.1, pp. 94–106. ISSN: 0169-555X. DOI: [10.1016/J.GEOMORPH.2010.09.029](https://doi.org/10.1016/J.GEOMORPH.2010.09.029).
- Florinsky, Igor V. (2009). "Computation of the third-order partial derivatives from a digital elevation model". In: *International journal of geographical information science* 23.2, pp. 213–231. ISSN: 13658816. DOI: [10.1080/13658810802527499](https://doi.org/10.1080/13658810802527499). URL: <https://www.tandfonline.com/doi/abs/10.1080/13658810802527499>.
- Fulton, Robert J (1995). *Surficial materials of Canada / Matériaux superficiels du Canada*. DOI: <https://doi.org/10.4095/205040>. URL: <http://geoscan.ess.nrcan.gc.ca/cgi-bin/starfinder/0?path=geoscan.fl&id=fastlink&pass=&search=R=205040&format=FLFULL>.
- Fulton, Robert J and Victor K Prest (1987). "Introduction: The Laurentide Ice Sheet and its Significance". In: *Géographie physique et Quaternaire* 41.2, pp. 181–186. URL: <https://id.erudit.org/iderudit/032676ar>.



- Gallant, John C. and John P. Wilson (1996). "TAPES-G: A grid-based terrain analysis program for the environmental sciences". In: *Computers & Geosciences* 22.7, pp. 713–722. ISSN: 0098-3004. DOI: [10.1016/0098-3004\(96\)00002-7](https://doi.org/10.1016/0098-3004(96)00002-7).
- Gauss, Carolo Friderico (1828). "Disquisitiones generales circa superficies curvas". In: *Commentationes societatis regiae scientiarum Gottingensis recentiores, Commentationes classes mathematicae* 1.
- Gowan, Evan J. et al. (2019). "Geology datasets in North America, Greenland and surrounding areas for use with ice sheet models". In: *Earth System Science Data* 11.1, pp. 375–391. ISSN: 18663516. DOI: [10.5194/ESSD-11-375-2019](https://doi.org/10.5194/ESSD-11-375-2019).
- Hengl, Tomislav and Hannes I Reuter (2009). *Geomorphometry - Concepts, Software, Applications*. Elsevier.
- Jasiewicz, Jarosław and Tomasz F. Stepinski (2013). "Geomorphons-a pattern recognition approach to classification and mapping of landforms". In: *Geomorphology* 182, pp. 147–156. ISSN: 0169555X. DOI: [10.1016/J.GEOMORPH.2012.11.005](https://doi.org/10.1016/J.GEOMORPH.2012.11.005). URL: <http://dx.doi.org/10.1016/j.geomorph.2012.11.005>.
- Jorge, Marco G. and Tracy A. Brennand (July 2017). "Semi-automated extraction of longitudinal subglacial bedforms from digital terrain models – Two new methods". In: *Geomorphology* 288, pp. 148–163. ISSN: 0169-555X. DOI: [10.1016/J.GEOMORPH.2017.04.001](https://doi.org/10.1016/J.GEOMORPH.2017.04.001).
- Lacelle, Denis et al. (Sept. 2018). "Buried remnants of the Laurentide Ice Sheet and connections to its surface elevation". In: *Scientific Reports* 8.1, pp. 1–10. ISSN: 2045-2322. DOI: [10.1038/s41598-018-31166-2](https://doi.org/10.1038/s41598-018-31166-2). URL: <https://www.nature.com/articles/s41598-018-31166-2>.
- Lewington, Emma L.M., Stephen J. Livingstone, Chris D. Clark, et al. (2020). "A model for interaction between conduits and surrounding hydraulically connected distributed drainage based on geomorphological evidence from Keewatin, Canada". In: *Cryosphere* 14.9, pp. 2949–2976. ISSN: 19940424. DOI: [10.5194/TC-14-2949-2020](https://doi.org/10.5194/TC-14-2949-2020).
- Lewington, Emma L.M., Stephen J. Livingstone, Andrew J. Sole, et al. (2019). "An automated method for mapping geomorphological expressions of former subglacial meltwater pathways (hummock corridors) from high resolution digital elevation data". In: *Geomorphology* 339, pp. 70–86. ISSN: 0169-555X. DOI: [10.1016/J.GEOMORPH.2019.04.013](https://doi.org/10.1016/J.GEOMORPH.2019.04.013).
- MacMillan, R. A. and P. A. Shary (2009). "Landforms and Landform Elements in Geomorphometry". In: *Developments in Soil Science*. Vol. 33. C, pp. 227–254. DOI: [10.1016/S0166-2481\(08\)00009-3](https://doi.org/10.1016/S0166-2481(08)00009-3).
- Maxwell, J. Clerk (1870). "L. On hills and dales". In: *The London, Edinburgh, and Dublin Philosophical Magazine and Journal of Science* 40.269, pp. 421–427. ISSN: 1941-5982. DOI: [10.1080/14786447008640422](https://doi.org/10.1080/14786447008640422).
- Meddens, Arjan J.H. et al. (2018). "Developing 5m resolution canopy height and digital terrain models from WorldView and ArcticDEM data". In: *Remote Sensing of Environment* 218, pp. 174–188. ISSN: 00344257. DOI: [10.1016/j.rse.2018.09.010](https://doi.org/10.1016/j.rse.2018.09.010). URL: <https://doi.org/10.1016/j.rse.2018.09.010>.


- Nye, J. F. (1965). “The Flow of a Glacier in a Channel of Rectangular, Elliptic or Parabolic Cross-Section”. In: *Journal of Glaciology* 5.41, pp. 661–690. ISSN: 0022-1430. DOI: [10.3189/s0022143000018670](https://doi.org/10.3189/s0022143000018670).
- Olaya, V. (2009). “Basic Land-Surface Parameters”. In: *Developments in Soil Science*. Vol. 33. C, pp. 141–169. DOI: [10.1016/S0166-2481\(08\)00006-8](https://doi.org/10.1016/S0166-2481(08)00006-8).
- Penck, Albrecht (1894). *Morphologie der Erdoberfläche*. Vol. 1. Stuttgart: Engelhorn.
- PGC (2021). *ArcticDEM – Polar Geospatial Center*. URL: <https://www.pgc.umn.edu/data/arcticdem/>.
- Pike, R.J. (1988). “The geometric signature: Quantifying landslide-terrain types from digital elevation models”. In: *Mathematical Geology* 20.5, pp. 491–511. ISSN: 08828121. DOI: [10.1007/BF00890333](https://doi.org/10.1007/BF00890333).
- Pike, R.J., I.S. Evans, and T. Hengl (2009). “Geomorphometry: A Brief Guide”. In: *Developments in Soil Science*. Vol. 33, pp. 3–30. ISBN: 978-0-12-374345-9.
- Porter, Claire et al. (2018). *ArcticDEM – Polar Geospatial Center*. DOI: <https://doi.org/10.7910/DVN/OHHUKH>. URL: <https://www.pgc.umn.edu/data/arcticdem/>.
- Prest, V., D. Grant, and V. Rampton (1968). *New Glacial Map of Canada*. DOI: <https://doi.org/10.4095/108979>. URL: <https://geoscan.nrcan.gc.ca/starweb/geoscan/servlet.starweb?path=geoscan/fulle.web&search1=R=108979>.
- Puliti, Stefano et al. (2020). “Modelling above-ground biomass stock over Norway using national forest inventory data with ArcticDEM and Sentinel-2 data”. In: *Remote Sensing of Environment* 236, p. 111501. ISSN: 00344257. DOI: [10.1016/j.rse.2019.111501](https://doi.org/10.1016/j.rse.2019.111501). URL: <https://doi.org/10.1016/j.rse.2019.111501>.
- Reuter, H. I. et al. (Jan. 2009). “Preparation of DEMs for Geomorphometric Analysis”. In: *Developments in Soil Science*. Vol. 33. C. Elsevier, pp. 87–120. DOI: [10.1016/S0166-2481\(08\)00004-4](https://doi.org/10.1016/S0166-2481(08)00004-4).
- Riley, Shawn J and Stephen Daniel Degloria (1999). “A Terrain Ruggedness Index that Quantifies Topographic Heterogeneity”. In: *Reprinted from: Intermountain Journal of Science* 5.1-4, pp. 23–27. URL: <https://www.researchgate.net/publication/259011943>.
- Röthlisberger, Hans (1972). “Water Pressure in Intra- and Subglacial Channels”. In: *Journal of Glaciology* 11.62, pp. 177–203. ISSN: 0022-1430. DOI: [10.3189/s0022143000022188](https://doi.org/10.3189/s0022143000022188).
- SETSM by MJ Remote Sensing* (n.d.). URL: <https://mjremotesensing.wordpress.com/setsm/>.
- Shary, Peter A., Larisa S. Sharaya, and Andrew V. Mitusov (2002). “Fundamental quantitative methods of land surface analysis”. In: *Geoderma* 107.1-2, pp. 1–32. ISSN: 00167061. DOI: [10.1016/S0016-7061\(01\)00136-7](https://doi.org/10.1016/S0016-7061(01)00136-7).
- Shreve, R. L. (1972). “Movement of Water in Glaciers”. In: *Journal of Glaciology* 11.62, pp. 205–214. ISSN: 0022-1430. DOI: [10.3189/s002214300002219x](https://doi.org/10.3189/s002214300002219x).
- Storrar, Robert D., A. Jones, et al. (2021). “Ice sheet scale subglacial meltwater conduit dimensions and processes: insights from 3D morphometry of a large sample of eskers”. In: *EGU General Assembly*. URL: <https://doi.org/10.5194/egusphere-egu21-11371>.

- Storrar, Robert D., Chris R. Stokes, and David J.A. Evans (2013). “A map of large Canadian eskers from Landsat satellite imagery”. In: *Journal of Maps* 9.3, pp. 456–473. ISSN: 17445647. DOI: [10.1080/17445647.2013.815591](https://doi.org/10.1080/17445647.2013.815591).
- (2014a). “Increased channelization of subglacial drainage during deglaciation of the laurentide ice sheet”. In: *Geology* 42.3, pp. 239–242. ISSN: 00917613. DOI: [10.1130/G35092.1](https://doi.org/10.1130/G35092.1).
- (2014b). “Morphometry and pattern of a large sample (>20,000) of Canadian eskers and implications for subglacial drainage beneath ice sheets”. In: *Quaternary Science Reviews* 105, pp. 1–25. ISSN: 02773791. DOI: [10.1016/j.quascirev.2014.09.013](https://doi.org/10.1016/j.quascirev.2014.09.013).
- Straumann, Ralph (2010). “Extraction And Characterisation Of Landforms From Digital Elevation Models: Fiat Parsing The Elevation Field”. PhD thesis. University of Zurich.
- Straumann, Ralph and Ross S. Purves (2008). “Delineation of valleys and valley floors”. In: *International Conference on Geographic Information Science*. Berlin, Heidelberg: Springer, pp. 320–336.
- Susan Mayhew, ed. (2015). *Search Results for esker*. Oxford Reference: A Dictionary of Geography. URL: <https://www.oxfordreference.com/search?source=%2F10.1093%2Facref%2F9780199680856.001.0001%2Facref-9780199680856&q=esker>.
- Weibel, Robert and J S DeLotto (1988). “Automated terrain classification for GIS modeling”. In: *GIS/LIS'88 Proceedings*. San Antonio, TX (USA), pp. 618–627.
- Wood, J.D. (1996). “The geomorphological characterisation of digital elevation models”. PhD thesis. University of Leicester. DOI: [10.1016/S0065-230X\(09\)04001-9](https://doi.org/10.1016/S0065-230X(09)04001-9). URL: <http://www soi.city.ac.uk/~jwo/phd>.
- Wu, Qiang, Fatima Aziz Merchant, and Kenneth R. Castleman (2008). *Microscope image processing*. Elsevier. ISBN: 9780080558547.
- Zevenbergen, Lyle W. and Colin R. Thorne (1987). “Quantitative analysis of land surface topography”. In: *Earth Surface Processes and Landforms* 12.1, pp. 47–56. ISSN: 1096-9837. DOI: [10.1002/ESP.3290120107](https://doi.org/10.1002/ESP.3290120107). URL: <https://onlinelibrary.wiley.com/doi/full/10.1002/esp.3290120107%20https://onlinelibrary.wiley.com/doi/abs/10.1002/esp.3290120107%20https://onlinelibrary.wiley.com/doi/10.1002/esp.3290120107>.

## Personal Declaration

I declare that this thesis has been composed solely by myself. Except where states otherwise by reference or acknowledgment, the work presented is entirely my own. The thesis has not been submitted, in whole or in part, in any previous application for a degree or in order to obtain ECTS points at any institution of higher education.

Zurich, 31 March 2022  
.....  
Place, Date

  
.....  
Signature of the author